Journal of Structural Geology 84 (2016) 47–67

Contents lists available at ScienceDirect

Journal of Structural Geology

journal homepage: www.elsevier.com/locate/jsg

Cycles of passive versus active diapirism recorded along an exposed salt wall

G.I. Alsop [a, *], R. Weinberger [b, c], T. Levi [b], S. Marco [d]

[a] Department of Geology and Petroleum Geology, School of Geosciences, University of Aberdeen, Aberdeen, UK
[b] Geological Survey of Israel, Jerusalem, Israel
[c] Department of Geological and Environmental Sciences, Ben Gurion University of the Negev, Beer Sheva, Israel
[d] Department of Geosciences, Tel Aviv University, Israel

ARTICLE INFO

Article history:
Received 7 November 2015
Received in revised form
14 January 2016
Accepted 26 January 2016
Available online 29 January 2016

Keywords:
Salt
Diapirism
Salt wall
Unconformities
Halokinetic sequences
Dead sea

ABSTRACT

Although it has long been recognised that passive salt diapirism may encompass sub-ordinate cycles of active diapirism, where sedimentary overburden is periodically shed off the roof of the rising salt, there has been very little study of this process around exposed salt (halite) diapirs. However, the Late Miocene-Pliocene Sedom salt wall, on the western side of the Dead Sea Basin, presents an opportunity for detailed outcrop analysis of diapiric salt and the associated depositional and deformational record of its movement during both passive and active phases of diapirism. The sub-seismic scale record of diapirism includes sedimentary breccia horizons interpreted to reflect sediments being shed off the crest of the growing salt wall, together with exceptional preservation of rotated unconformities and growth faults. Areas of more pronounced dips directed towards the salt wall are capped by unconformities, and interpreted to represent withdrawal basins within the overburden that extend for at least 1500 m from the salt margin. Elsewhere, broad areas of upturn directed away from the salt extend for up to 1250 m and are marked by a sequence of rotated unconformities which are interpreted to bound halokinetic sequences. The margins of the salt wall are defined by steep extensional boundary faults that cut upturned strata, and have enabled rapid and active uplift of the salt since the Holocene. The Sedom salt wall therefore charts the transition from passive growth marked by withdrawal basins, growth faults and unconformities, to more active intrusion associated with major boundary faults that enable the rapid uplift of overburden deposited on top of the salt to ~100 m above regional elevations in the past 43 ka. Individual cycles of passive and active diapirism occur over timescales of <30 ka, which is up to an order of magnitude less than typically suggested for other settings, and highlights the dynamic interplay between salt tectonics and sedimentation in an environment undergoing rapid fluctuations in water level.

1. Introduction

It has long been recognised that the sedimentary overburden which surrounds salt structures provides a detailed record for the nature and timing of adjacent salt flow and diapirism (e.g. Trusheim, 1960). However, owing to the extreme aridity required to preserve halite at the earth's surface, the study of salt tectonics suffers from a “scarcity and poor quality of field exposures” (Ringenbach et al., 2013). In recent decades, much of the research effort on salt tectonics has therefore focussed on physical modelling (e.g. Hudec and Jackson, 2011; Dooley et al., 2015), numerical modelling (e.g. Fuchs et al., 2014, 2015) and numerous studies involving the interpretation of seismic sections through salt-influenced basins (e.g. Archer et al., 2012; Jackson et al., 2014, 2015). However, the often steep attitude of bedding adjacent to salt structures, coupled with complications associated with stratigraphic facies changes, and increased faulting and fluid flow concentrated along salt margins, can hinder seismic analysis (see Davison et al., 2000a, b). Direct observations on salt and the adjacent overburden have been largely restricted to a few areas such as the Zagros Mountains (e.g. Talbot, 1979, 1998; Aftabi et al., 2010) which are complicated by ongoing orogenesis, or underground mine workings that, owing to their economic drivers, are focussed on the salt itself rather than the surrounding overburden (e.g. Schofield et al., 2014; Burliga, 2014). Although modelling, seismic

* Corresponding author.
E-mail address: Ian.Alsop@abdn.ac.uk (G.I. Alsop).

http://dx.doi.org/10.1016/j.jsg.2016.01.008
0191-8141/

interpretation and mine studies each generate important information regarding salt tectonics, they suffer from a collective weakness to deliver detailed (sub-seismic scale) structural and sedimentary observations from overburden surrounding the salt. Our scientific motivation is therefore to provide a detailed analysis of the evolution of a diapiric salt wall based on direct observations of outcrops of halite and adjacent sediments. The outcrop study of halite-rich structures is important because salt diapirs dominated by, or containing other evaporitic minerals such as gypsum may display different seismic attributes (e.g. Vargas-Meleza et al., 2015) and/or structural architectures. This point has recently been emphasised by Butler et al. (2015) who note that "shallowly buried gypsum need not form a weak layer within sedimentary successions, which may be important when considering mobilization of evaporite successions soon after their deposition".

Diapiric salt that cross cuts the adjacent sedimentary overburden may either form broadly cylindrical bodies termed salt stocks where the cross sectional ratio is <2, or linear salt walls defined as where the ratio is >2 (Hudec and Jackson, 2011, p.31). Active salt diapirism may simply be defined as "diapir rise by arching, uplifting, or shouldering aside it's roof" (Hudec and Jackson, 2011, p269). Halokinetic active diapirism is driven by overburden load, causing diapiric salt to be pressurised and exert an upward force on its roof. If this buoyancy force is greater than the strength of the roof, then the roof is pushed up as the diapir actively rises (Hudec and Jackson, 2011, p269) (Fig. 1a). Active diapirs are typically marked by: i) stratigraphic units being lifted above their regional elevations on the diapiric crest, ii) normal faulting and grabens forming in sediments over the diapiric crest, iii) large boundary faults permitting the relative rise of salt along the diapiric flanks, and iv) a lack of significant facies change in surrounding sediments (e.g. Nelson, 1991; Schultz-Ela et al., 1993; Rowan, 1995, p.204) (Fig. 1a).

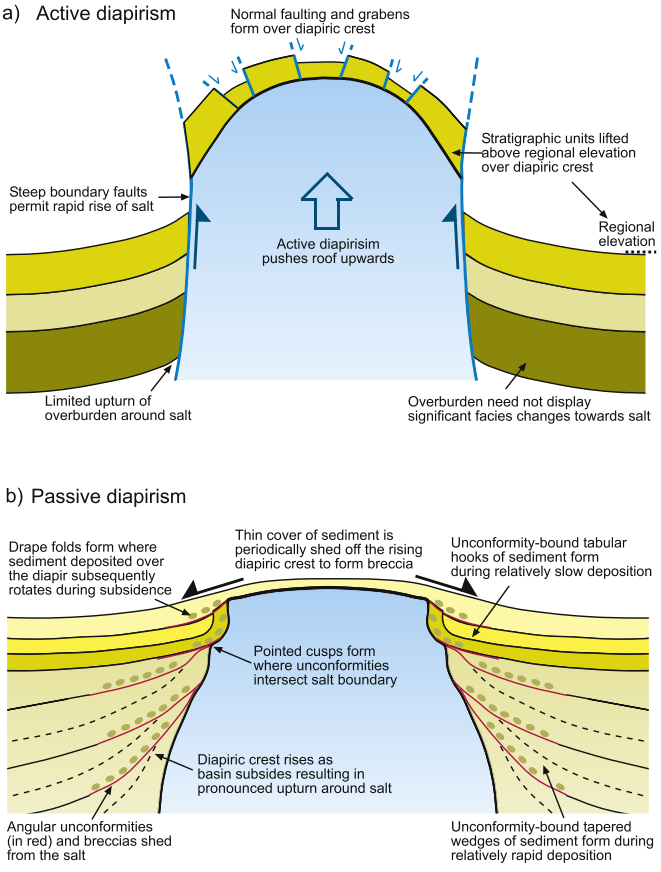

Fig. 1. Schematic cartoons illustrating typical features of a) active salt diapirism and, b) passive salt diapirism.

Passive salt diapirism is defined as "syndepositional growth of a diapir whose exposed crest rises as sediments accumulate around it" (Hudec and Jackson, 2011, p.275). In passive diapirism, the diapir crest can be occasionally buried, but the diapir repeatedly breaks through the thin temporary roof strata. The base of the salt continues to subside with the basin as it fills with sediment, while the crest of the diapir keeps pace with sedimentation in a 'down-building' process (e.g. Vendeville and Jackson, 1991; Hudec and Jackson, 2011 p.275) (Fig. 1b). Passive diapirs are typically associated with: i) pronounced areas of bedding upturn, ii) sedimentary facies changes, and iii) unconformities and breccia horizons within overburden around the flanks of the diapir (Fig. 1b). There is therefore a distinct stratigraphic and sedimentological record of salt movement during passive diapirism. Criteria for recognising passive and active diapirs have been previously summarised by Jackson et al. (1994), Rowan (1995) and Davison et al. (2000a, b).

Bedding upturn and folding noted above is attributed to the shearing of rocks and sediments around the diapir as the salt rises and/or the sediments sink, and may be generated via the passive rise or active piercement of salt (Bornhauser, 1969; Alsop et al., 2000; Davison et al., 2000a, b; Rowan et al., 2003). Drape folding is specifically created where sediments are deposited directly over the flanks of a growing salt diapir, and are subsequently rotated into steeper attitudes as the sediments sink around the salt during passive diapirism (Schultz-Ela, 2003; Rowan et al., 2003; Giles and Rowan, 2012) (Fig. 1b). Drape folding is therefore a near surface process that occurs by "rotation of beds in and below the bathymetric scarp" marking the passive diapir (Rowan et al., 2003, p.753). Rowan et al. (2003, p.753) note however, that "passive diapirism actually entails cycles of small-scale active diapirism as the salt periodically inflates and lifts a thin cover during times of slow sedimentation" (see also Hearon et al., 2014, p.58; Salazar et al., 2014). Davison et al. (1996a, p.8) suggest that this cover will typically be <50 m in thickness. Given that cycles of both passive and active diapirism may therefore occur, the question becomes one of determining the relative components of each, and the contribution that each makes to the deposition and deformation of sediments during the growth of an individual diapir.

There are very few outcrop-based studies of the structural and sedimentological effects of salt diapirs, where halite is actually exposed at the earth's surface. The classic work of Rowan et al. (2003) and Giles and Rowan (2012) on La Popa in Mexico is in an area that has suffered subsequent contraction and lacks halite exposures. The preliminary work of Li et al. (2014) in a newly recognised salt tectonic province in NW China records a very thin (<50 m wide) salt wall where halite is exposed at the surface, but which is overprinted by a regional fold and thrust belt. The recent studies of halokinetic sequences in the Sivas Basin in Turkey (Ringenbach et al., 2013; Callot et al., 2014), together with the work of Poprawski et al. (2014) in northern Spain are marked by evaporites being dominated by gypsum (rather than halite) and also suffer from salt-related structures being overprinted by later regional contraction. Despite this welcome surge in recent publications focussing on outcrop studies of salt tectonics, there still remains a lack of detailed work on exposures of halite-dominated diapirs that have not suffered overprinting by contraction and orogenesis.

As discussed by Alsop et al. (2015) the Sedom salt wall on the western margin of the exceptionally arid Dead Sea Basin (Fig. 2a, b) receives <50 mm precipitation per year and has the advantage over many areas in that a) halite and surrounding clastic overburden are

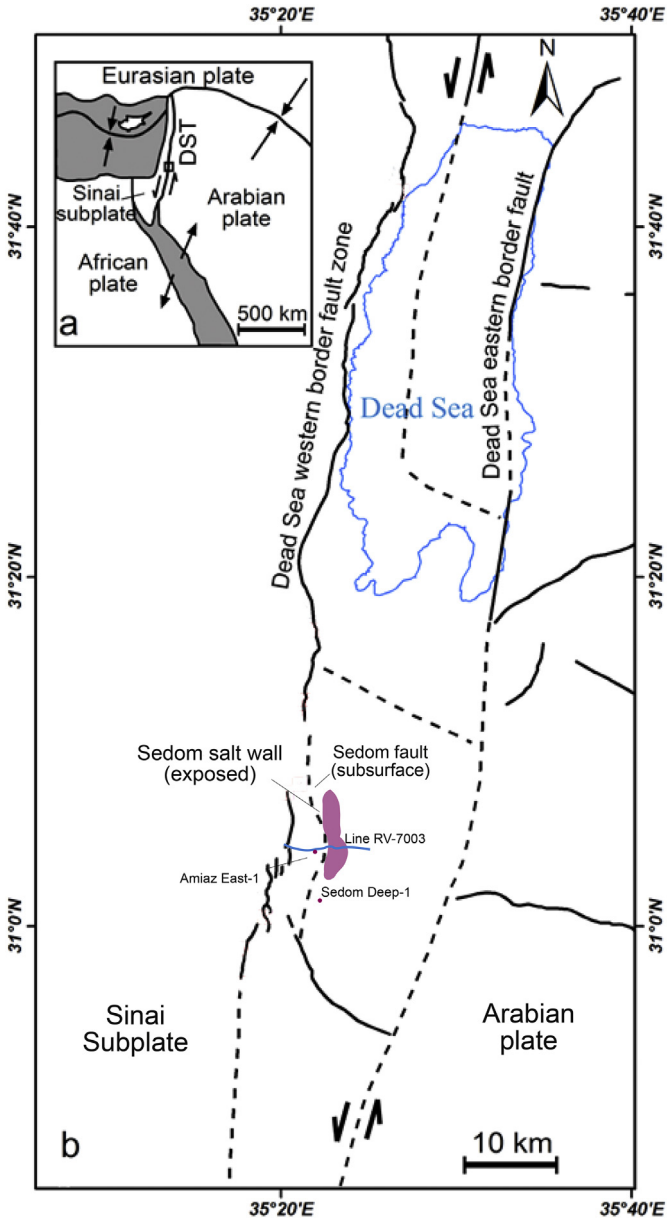

Fig. 2. a) Tectonic plates in the Middle East. General tectonic map showing the location of the present Dead Sea Fault (DSF). The Dead Sea Fault is a left-lateral fault between the Arabian and African (Sinai) plates that transfers the opening motion in the Red Sea to the Taurus – Zagros collision zone with the Eurasian plate. Location of b) shown by the small box on the DSF. b) Map of the Dead Sea showing the position of the exposed Sedom salt wall and strands of the Dead Sea Fault (based on Sneh and Weinberger, 2014). The locations of the RV-7003 seismic line, together with the Sedom Deep-1 and Amiaz East-1 boreholes are shown, as is the subsurface trace of the Sedom Fault. (For interpretation of the references to colour in this figure legend, the reader is referred to the web version of this article.)

well preserved at outcrop; b) there are a range of mixed evaporites that enable a greater understanding of internal diapiric processes; c) the Late Miocene-Pliocene salt is relatively young and still rising, thereby allowing a greater appreciation of factors controlling its growth, d) the linear salt wall geometry has the potential to preserve geometries at different stages of development along its length; e) there is a large existing data base comprising detailed maps (e.g. Zak, 1967; Agnon et al., 2006), isotopic dating (e.g. Torfstein et al., 2009; Matmon et al., 2014), mechanical analysis (e.g. Hatzor and Heyman, 1997), palaeomagnetic studies (e.g. Weinberger et al., 1997), and InSAR (e.g. Weinberger et al., 2006a, b).

In this case study we use the Sedom salt wall to raise a number of research questions relating to the geometry and extent of deformation in overburden adjacent to diapirs that have undergone both passive growth and active piercement including:

a) What is the geometry and extent of bedding upturn adjacent to a salt margin?
b) What is the geometry and extent of unconformities adjacent to a salt margin?
c) At what depth does upturned bedding develop adjacent to a salt margin?
d) Is deformation concentrated along unconformites adjacent to a salt margin?
e) How is diapiric uplift achieved without widespread deformation adjacent to a salt margin?
f) What are the rates and durations of diapiric cycles recorded adjacent to a salt margin?

Thus, our field-based approach aims to provide a better understanding of the detailed stratigraphic and structural relationships within and around salt diapirs that would normally be lost as they are below the limits of seismic resolution. This ultimately allows us to more rigorously test salt tectonic models with obvious implications for hydrocarbon exploration.

2. Overview of the Sedom salt wall and associated basin evolution

2.1. Sedom salt wall – passive versus active diapirism

The Sedom salt wall is a ~10 km long N–S trending ridge that rises ~240 m above the level of the Dead Sea (Fig. 2a, b, 3a, b). Contrary to many studies of salt diapirs noted above, the Sedom salt wall has not suffered later contractional deformation as it is located in a releasing bend of the left-lateral NNE-SSW trending Dead Sea Fault (e.g. Garfunkel, 1981; Smit et al., 2008) (Fig. 2b). In general, the releasing bends of strike-slip fault systems form ideal locations for the development of salt diapirs as overburden is weakened by extensional faulting and fracturing (e.g. Fossen, 2010, p.389). In detail, the Sedom salt wall is commonly divided into northern and southern segments, each of which is ~4 km long and ~1.5–2 km wide at surface (Fig. 3a, b). These two segments are separated from one another by a 2 km long central 'pinched' section where the margins of the wall converge and its width reduces to just ~800 m. The western margin of the Sedom wall dips moderately to steeply towards the west, while the eastern flank also dips variably towards the west and is overturned (see Alsop et al., 2015). The northern limit of the Sedom salt wall is marked by moderate dips towards the north, where the 'nose' of the salt wall plunges below the surrounding overburden (Fig. 3a, b). Seismic profiles across the salt wall suggest that it is located adjacent to the underlying Sedom Fault, a major ~ N–S trending extensional fault that may have focussed the upward flow of salt from depths of 3–4 km (Gardosh et al., 1997; Weinberger et al., 2006a) (Fig. 2b).

Throughout much of its history, the Sedom salt wall has undergone passive diapirism driven by positive buoyancy linked to the thick accumulation of >5500 m of Plio-Pleistocene overburden sediments directly to the east in the southern Dead Sea Basin (Al-Zoubi and ten Brink, 2001; Weinberger et al., 2006a; Alsop et al., 2015). However, it has also been noted that the Sedom salt wall has previously undergone periods of "forceful intrusion" and "active-style diapirism" during its growth (e.g. Weinberger et al., 2006a, p.39, 47). This diapiric growth has led to sediment being periodically shed off the crest of the rising salt wall, resulting in sedimentary breccias marking local, rotated unconformities

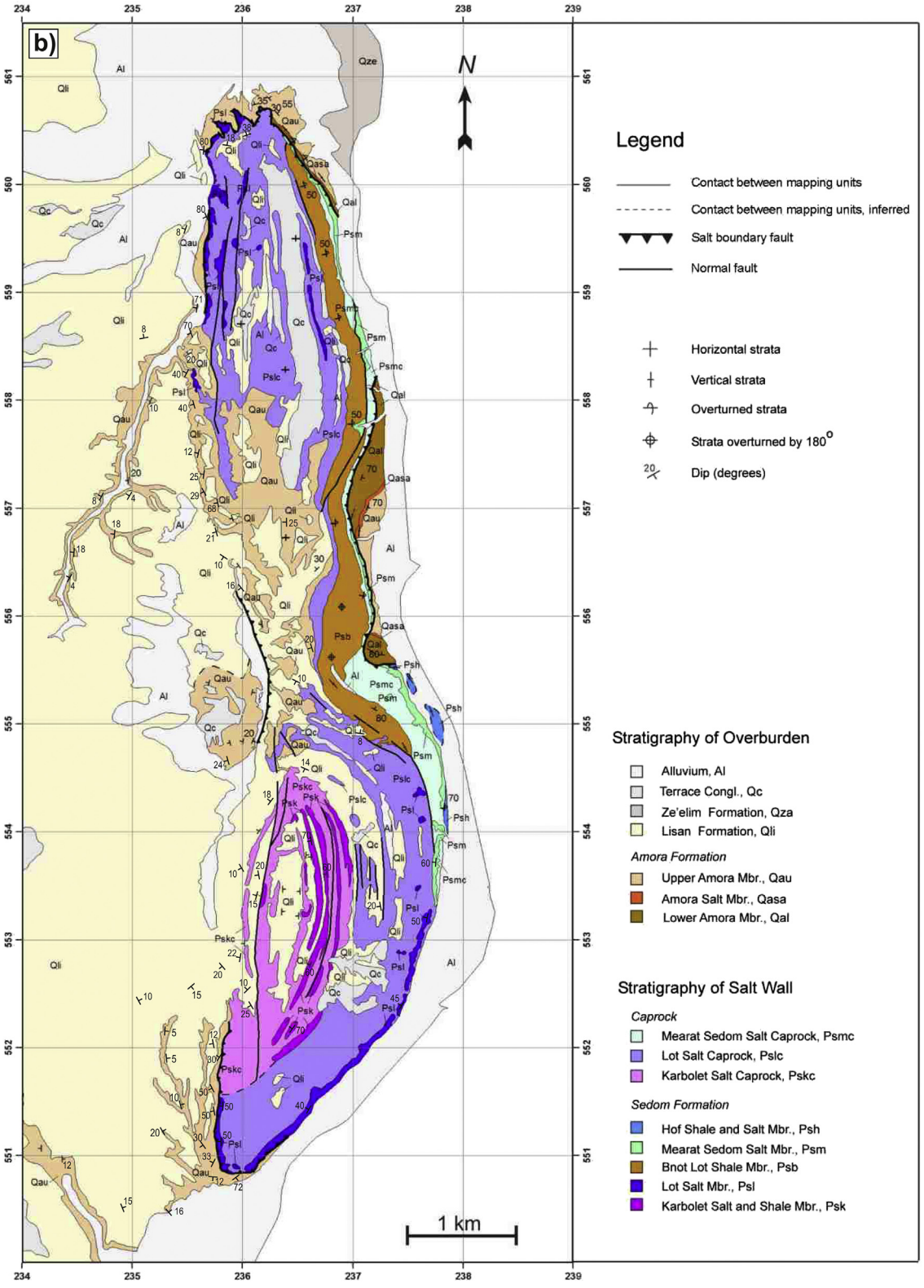

Fig. 3. a) Overview photograph of the Sedom salt wall forming a 10 km long N–S trending ridge rising above the Amiaz plain. b) Geological map of the Sedom salt wall and adjacent sedimentary overburden based on Zak (1967) and Agnon et al. (2006). The area of interest in this study is the western flank of the Sedom salt wall. See Fig. 2b for location.

immediately to the west and east of the Sedom salt wall (Weinberger et al., 2006a, b; Alsop et al., 2015). The Sedom salt wall is presently undergoing a phase of active diapirism as demonstrated by a broad range of criteria:

a) The thin sedimentary roof overlying the Sedom salt wall comprises the Lisan Formation (Table 1) which has been dated as 43 ka and has been uplifted by ~100 m above its regional elevation. The top of this unit has been dated as 15.5 ka and has risen 75 m above its regional elevation, indicating average uplift rates of 5 mm/year (see Weinberger et al., 2006a).
b) A fossilised dissolution surface termed the 'salt mirror' (e.g. Farkash et al., 1951; Zak and Freund, 1980) was created when Dead Sea water levels dropped at 14–11 ka (Weinberger et al., 2006a). This originally flat surface has been subsequently uplifted by 80 m across faults bounding the eastern salt margin, providing an average uplift rate of between 5.5 and 11 mm/year (Weinberger et al., 2006a; Zucker, 2014).
c) Karstic weathering of the Sedom salt wall results in caves and subterranean passages, which were left hanging 'high and dry' 46 m above the current channel as the salt rose by up to 6–7 mm/year during the last 8 ka (Frumkin, 1996a, b, c).
d) Active uplift of the Sedom salt wall results in a topographic ridge that blocks modern drainage patterns, deflecting incised wadis to both the north and south of the salt wall, and preventing run-off directly towards the basin.
e) InSAR analysis reveals current uplift rates in the order of 5.5–8 mm/year over large areas along the crest of the Sedom salt wall (Weinberger et al., 2006b).
f) Major boundary faults are developed along the flanks of the salt wall (e.g. Zak, 1967; Weinberger et al., 2006a) and permit the rapid rise of salt noted above.
g) Extensional faults define grabens in sediments preserved above the crest of the salt wall (e.g. Zak, 1967).

All of these observations indicate that the Sedom salt wall is currently undergoing a phase of active diapirism, within a longer record of generally passive growth. As such, it presents an ideal opportunity to undertake an outcrop study of halite and surrounding clastic sediments that record the repeated transitions from passive to active diapirism in a non-contractional setting. Such opportunities are exceptionally rare, and enable us to directly compare our observations with models that focus more on the 'downbuilding' phase of passive diapirism (e.g. Rowan et al., 2003; Giles and Rowan, 2012).

2.2. Basin evolution and stratigraphy

The Sedom salt wall is formed of the Sedom Formation predominantly comprising evaporites (75%) including halite, anhydrite and thin dolomites, interbedded with thinner clastic beds formed of siltstone, mudstone, clay and sandstones (Zak, 1967; Frumkin, 2009). The Sedom Formation is subdivided into five members, and incorporates the Bnot Lot Shales Member dated at 6.2 and 5.0 ± 0.5 Ma (Matmon et al., 2014; Zak, 1967) (Table 1).

This Late Miocene-Pliocene evaporite sequence penetrates the surrounding Pleistocene Amora and Lisan formations that form the overburden to the salt wall, via marginal faults and shear zones (Zak and Freund, 1980, Fig. 3b). The Amora Formation is subdivided into three members (Agnon et al., 2006, Table 1). The Lower Amora Member comprises 200 m of shales, sandstones and conglomerates and forms the lowest stratigraphic level exposed at outcrop dated at 740 ± 66 ka (U series ages from Torfstein et al., 2009). This is overlain by the Amora Salt Member which is a 10 m thick halite interval estimated via U–Th at 420 ± 10 ka (Torfstein et al., 2009). Finally, the 195 m thick Upper Amora Member comprising shales, sandstones and conglomerates sits stratigraphically above the salt member, and has been attributed a range of ages between 340 and 80 ka (Torfstein et al., 2009) at the PZ 2 borehole site (immediately west of Mount Sedom).

Although only 400–450 m of Amora Formation are actually exposed next to the Sedom salt wall, the overall Plio-Pleistocene sequence attains thicknesses of 5500 m in the southern Dead Sea Basin (Al-Zoubi and ten Brink, 2001; Weinberger et al., 2006a). Immediately to the SE of Sedom, the Sedom Deep-1 drill hole penetrated a 3700 m thick fluvio-lacustrine series which overlies a 900 m thick evaporite series (Figs. 2b and 3b). To the west of Mount Sedom, the Ami'az East-1 drill hole penetrated a 1300 m thick evaporite series overlain by a 1900 m thick clastic series (Weinberger et al., 2006a) (Figs. 2b and 3b). The base of the Lower Amora Member within the Ami'az East-1 borehole has been recently dated as 3.3 ± 0.9 Ma, while approximately 500 m stratigraphically higher, the Lower Amora sediments are dated as 2.7 ± 0.7 Ma (Matmon et al., 2014). Overall, the Sedom Formation thickens towards the depocentre and thins towards the western margin of the basin (e.g. Zak, 1967) (Figs. 2b and 3b). Salt flowing into the Sedom salt wall is considered to have been largely sourced from the east due to differential overburden loading, with

Table 1
Generalised stratigraphy and ages of the Sedom Formation that comprises the Sedom salt wall, and the Amora and Lisan Formations that form the overburden to the salt. Note that dissolution of salt members leads to local caprocks being preserved at the surface. TCN – Terrestrial cosmogenic nuclide burial ages.

Formation	Member	Description and age
Lisan formation		40 m of aragonite-rich lacustrine sediments dated between ~70 ka and 14 ka (U-series and ^{14}C, Kaufman, 1971; Haase-Schramm et al., 2004).
Amora Formation (overburden to Sedom salt wall)	Upper Amora Member	200 m of fluvio-lacustrine shales, sandstones and conglomerates ranging in age between 340 and 80 ka (Torfstein et al., 2009).
	Amora Salt Member	10 m thick halite unit dated at 420 ± 10 ka (U–Th ages from Torfstein et al., 2009)
	Lower Amora Member	200 m of fluvio-lacustrine shales, sandstones and conglomerates exposed at outcrop. Dated at 740 ± 66 ka (U series ages from Torfstein et al., 2009).
Sedom Formation (forms the Sedom salt wall)	Hof Shale and Salt Member	Up to 90 m of halite and shales (Zak et al., 1968)
	Mearat Sedom Salt Member	Up to 250 m of halite, anhydrite and minor clastics
	Bnot Lot Shales Member	Up to 200 m thick sandstones and shales dated at 6.2 and 5.0 ± 0.5 Ma (^{10}Be TCN burial ages from Matmon et al., 2014)
	Lot Salt Member	Up to 800 m of halite, anhydrite and minor clastics
	Karbolet Salt and Shale Member	550 m minimum thickness of halite and shale units (base not observed and not dated).

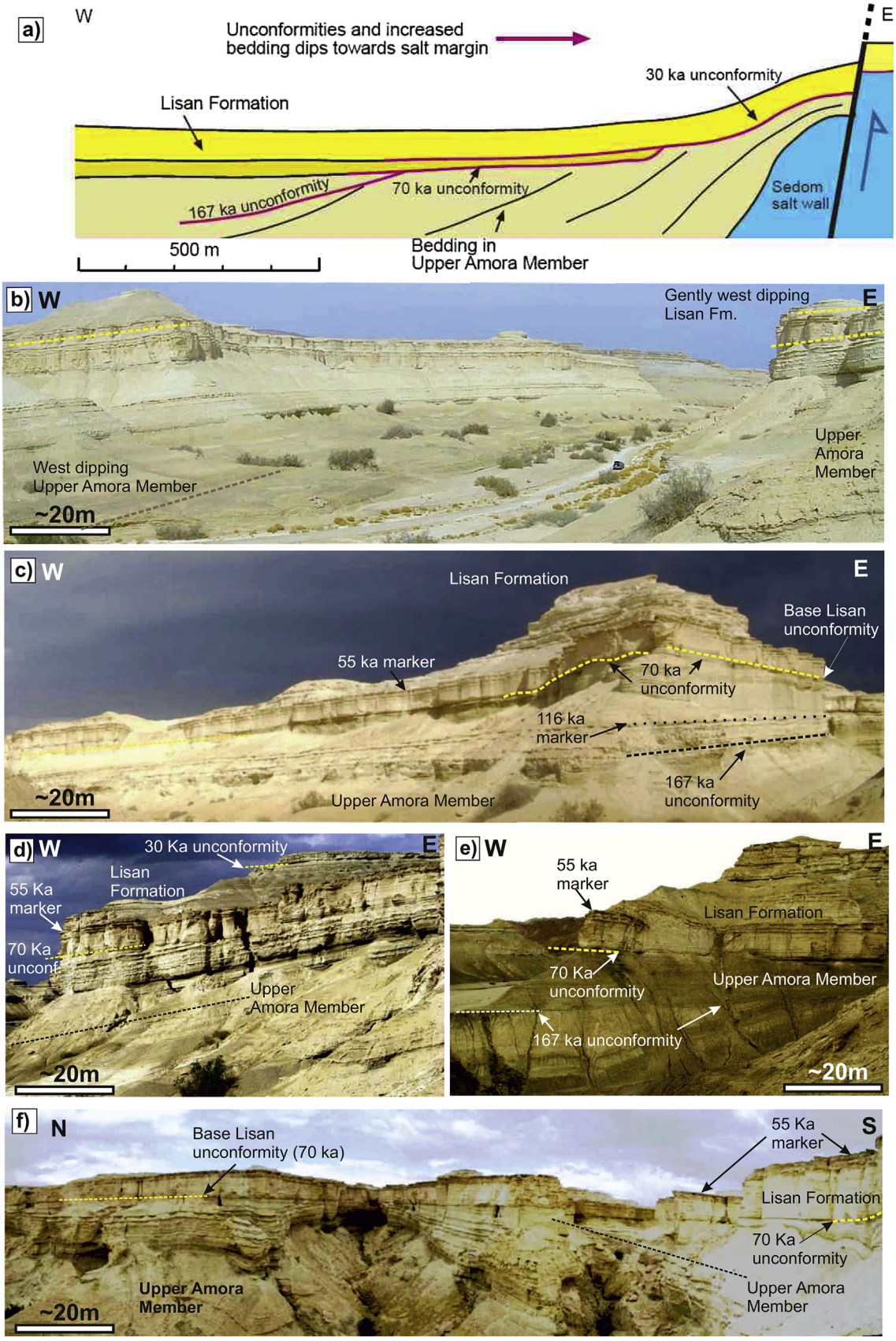

Fig. 4. a) Simplified W–E cross section across the NW flank of the Sedom salt wall (along Grid Northing 558 – see Fig. 3b). The cross section highlights increased bedding dips toward the salt wall, together with unconformities shown in photographs b–f). b–f) Photographs of unconformities and their approximate dates (from Waldmann et al., 2007) within the Upper Amora Member and overlying Lisan Formation from the NW flank of the Sedom salt wall. All photographs were taken within 100 m of (N31.10598°; E35.36660°) and are viewed with the salt margin towards the East (right) side of the photograph, apart from f) which is viewed looking directly towards the salt.

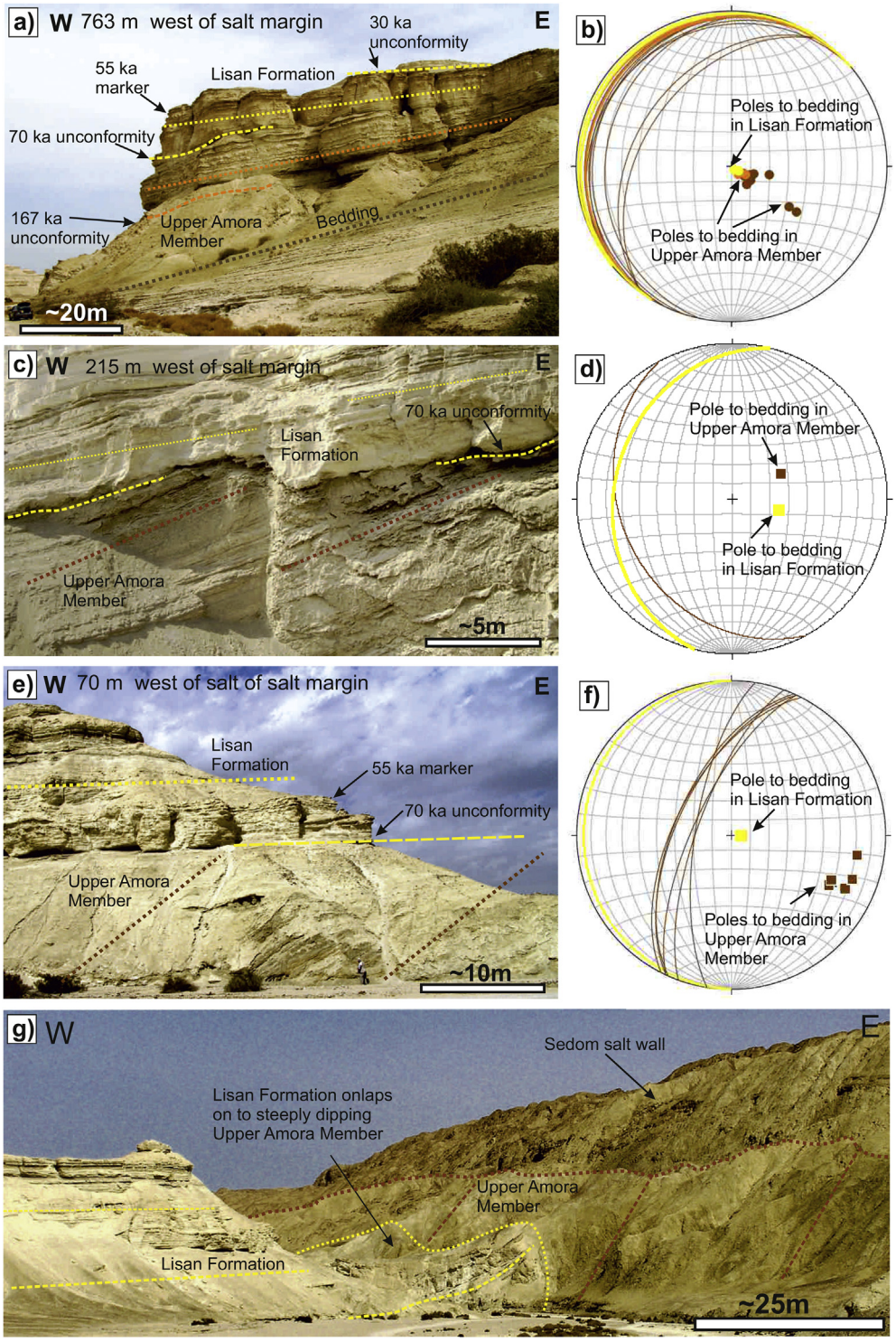

Fig. 5. Photographs (a, c, e, g) and associated stereonets (b, d, f) of upturned bedding and unconformities at various distances from the NW margin of the salt wall. Photographs a) and e) taken within 100 m of (N31.10598°; E35.36660°), while c) was taken at (N31°06′377″; E35°22′600″) and g) was taken at (N31°06′25.11″; E35°22′28.20″). All photographs were taken looking North with the salt margin towards the East (right) side of the photograph, In each case, bedding in the Upper Amora Member is shown in brown and orange, while bedding from the overlying Lisan Formation is highlighted in yellow. Unconformities within the Upper Amora Member and Lisan Formation are shown at a) 763 m, c) 215 m, e) 70 m, g) 0 m from the salt margin. Bedding is shown as both great circles and poles on the associated stereonets (b, d, f) and demonstrates how the obliquity along the angular unconformity between the Upper Amora Member and the Lisan Formation increases towards the salt margin. (For interpretation of the references to colour in this figure legend, the reader is referred to the web version of this article.)

only a minor component of salt derived from the west (Weinberger et al., 2006a). It is this component of flow that creates the structures and stratigraphy that we describe from the western flank of the Sedom salt wall.

The crest of the Sedom salt wall is covered by a 40 m thick insoluble caprock, which consists mainly of anhydrite, gypsum, as well as minor marl, clay, dolomite and sandstone fragments. The caprock is considered to have formed during dissolution of the

various salt members (Zak and Freund, 1980) during Upper Amora times (340–80 ka). The Pleistocene Lisan Formation overlies the Amora Formation and caprock, and consists of up to 40 m of aragonite-rich and detrital-rich laminae forming a varved lacustrine sequence, dated between ~70 ka and 14 ka by U-series and ^{14}C (Haase-Schramm et al., 2004, Table 1).

We now concentrate on the stratigraphic and structural evolution of the western flank of the Sedom salt wall. Although the Lower Amora Member has been proved by drilling at the Amiaz borehole (Fig. 2b), actual outcrops of overburden on the western flank of the salt wall are restricted to the Upper Amora Member and the overlying Lisan Formation which are now the focus of our attention.

3. Sedimentary and stratigraphic record of salt wall growth

3.1. Local angular unconformities associated with upturn of bedding towards the salt wall

It has long been recognised that sediments deposited against the flank of a rising salt diapir may be sequentially upturned and eroded to create local unconformities (e.g. Johnson and Bredeson, 1971; Alsop et al., 2000; Rowan et al., 2003; Hudec and Jackson, 2011, p. 78; Giles and Rowan, 2012) (Fig. 1b). The fold of sediment that is created over the diapiric flank may become over steepened and eventually undergo gravitational failure, resulting in an unconformity marking the erosional truncation of the upturned flap. Spectacular angular unconformities are indeed developed within and between the west-dipping Upper Amora Member and the overlying Lisan Formation exposed to the west of the Sedom salt wall (Fig. 4a–f). Following Alsop et al. (2000), we broadly divide areas of upturned bedding and associated unconformities around salt diapirs into 'outer' and 'inner' profiles based on the amount of upturn and deformation.

3.1.1. Unconformities – outer profile

At distances of 763 m from the diapiric contact, three distinct unconformities are exposed within the overburden (Figs. 4a–d, 5a, b, Table 2). Bedding in the Upper Amora Member dips at 24°W and is separated from overlying beds (mean 021/13W) by an angular unconformity dated at 167 ka (Bartov et al., 2002; Waldmann, 2002; Waldmann et al., 2007) (Fig. 4a, c, d, e, Table 2). The Upper Amora Member is truncated by an angular unconformity marking the base of the Lisan Formation dipping 040/7W and dated at 70 ka (Waldmann et al., 2007) (Figs. 4a and 5a, b). Finally, an unconformity dated at 30 ka (Bartov et al., 2002; Waldmann et al., 2007) also occurs within the Lisan Formation, with the upper sequence dipping 031/4W (Figs. 4a and 5a, b, Table 2). In addition, a marker bed within the Upper Amora Member has been dated by Waldmann et al. (2007) to 116 ka (Fig. 4c), while a distinctive 'triple gypsum' horizon within the Lisan Formation has been dated at 55 ka and acts as a useful stratigraphic guide around the flanks of the Sedom salt wall (Bartov et al., 2002; Waldmann et al., 2007, 2009).

3.1.2. Unconformities – inner profile

At 215 m from the diapir, the Upper Amora Member dips 152/29W, while the unconformably overlying Lisan Formation is oriented at 112/22S, generating an angular unconformity of 18° at the base of the Lisan Formation dated at 70 ka (Fig. 5c, d). At 70 m from the diapir, the Upper Amora Member is 020/60W, while the unconformably overlying Lisan Formation is oriented at 000/5W, generating an angular unconformity of ~50° at the base of the Lisan Formation (Fig. 5e, f). At 10 m the angular discordance has increased to 70°. The Upper Amora Member ultimately becomes steeply dipping on the NW flank of the salt wall, with the Lisan Formation displaying relatively gentle onlapping relationships directly onto the older unit (Figs. 4a and 5g).

3.2. Local angular unconformities associated with downturn of bedding towards the salt wall

The undisturbed Upper Amora Member and overlying Lisan Formation typically display very gentle (~1°) regional dips directed towards the east and the present depocentre of the Dead Sea Basin (e.g. Alsop and Marco, 2012a, b, 2013; 2014). However, at the extreme NW and SW margins of the Sedom salt wall, the Upper Amora Member and Lisan Formations locally display increased dips (up to 10°) directed towards the east.

At distances of 1500 m from the SW end of the Sedom salt wall, bedding within the Upper Amora Member dips gently towards the Sedom salt wall, and is unconformably overlain by sub-horizontal bedded Lisan Formation (Fig. 6a). At distances of 800 m from the salt, bedding within the Upper Amora Member dips at 16° toward the diapir, and is overlain via a marked angular unconformity by the sub-horizontal Lisan Formation (Fig. 6b, c). Steep SW-dipping growth faults within the Upper Amora Member are truncated by the erosive unconformity (Fig. 6d, e). At 70 m from the SW flank of the diapir, a series of rotated unconformities are observed within the Lisan Formation (Fig. 6f). Each unconformity appears to have been rotated down towards the diapir, before being unconformably capped by more gently dipping younger sequences.

3.3. Local conglomerates and breccias

Breccia horizons are sporadically developed within the Upper Amora Member along the western margin of the Sedom salt wall (Fig. 7a, b, c), and are similar to those described by Alsop et al. (2015) along the eastern flank of the diapir. Breccia clasts may reach 30 cm in length, are typically angular and comprise shales and sandstones (Fig. 7a). The friable and angular nature of clasts suggests that they would not survive transportation over significant distances, and are most likely sourced from sediments being shed off the growing salt wall (see Alsop et al., 2015).

Conglomerates are also locally preserved along the contact between the Upper Amora Member and overlying Lisan Formation about 70 m from the diapiric margin (Fig. 7d). Wedge-shaped fissures are sporadically developed along this contact, and locally contain rounded pebbles within them (Fig. 7d, e). This suggests possible emergence of the unconformity surface and neptunian

Table 2
Angles of tilt measured across dated unconformity surfaces at 763 m from exposed salt contact. Angles of tilt allow estimates of minimum net salt rise (R) and rates to be made.

	Unconformities at distance (d) 763 m from salt contact			
Age	167–70 ka	70–30 ka	30–0 ka	Total
Interval	97 ka	40 ka	30 ka	167 ka
Unconf. Tilt (α)	10°	7°	4°	21°
Net Salt Rise (R) R = d sin α	132.5 m	93 m	53 m	278.5 m
Salt rise/year	1.37 mm/a^{-1}	2.33 mm/a^{-1}	1.77 mm/a^{-1}	1.67 mm/a^{-1}

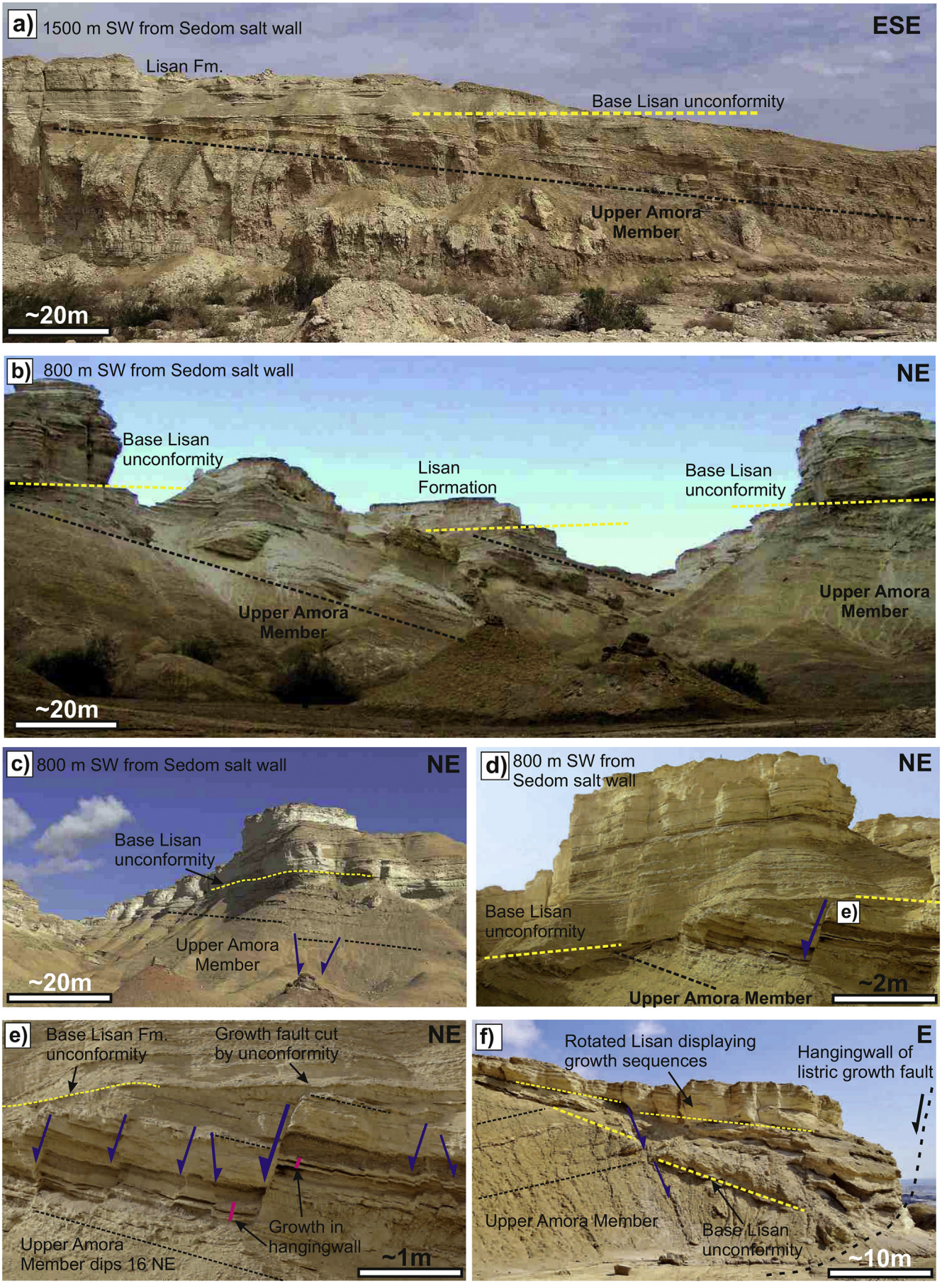

Fig. 6. a–e) Photographs of unconformities linked to downturn of bedding towards the SW margin of the Sedom salt wall. Bedding in the underlying Upper Amora Member consistently dips more steeply towards the salt than the overlying Lisan Formation. Photograph a) taken at (N31.044286°; E35.364665°). Extensional growth faults within the Upper Amora Member (d, e) are truncated by the base Lisan unconformity. Photographs b, c, d, e) taken at (N31.098697°; E35.361147°). f) Photograph (mirrored) of sedimentary growth packages and unconformities in the Lisan Formation that are progressively tilted towards the salt margin, in the hanging wall of a presumed listric growth fault (N31°03′32.30″; E35°22′32.32″). All photographs are viewed with the salt margin towards the East (right) side of the photograph.

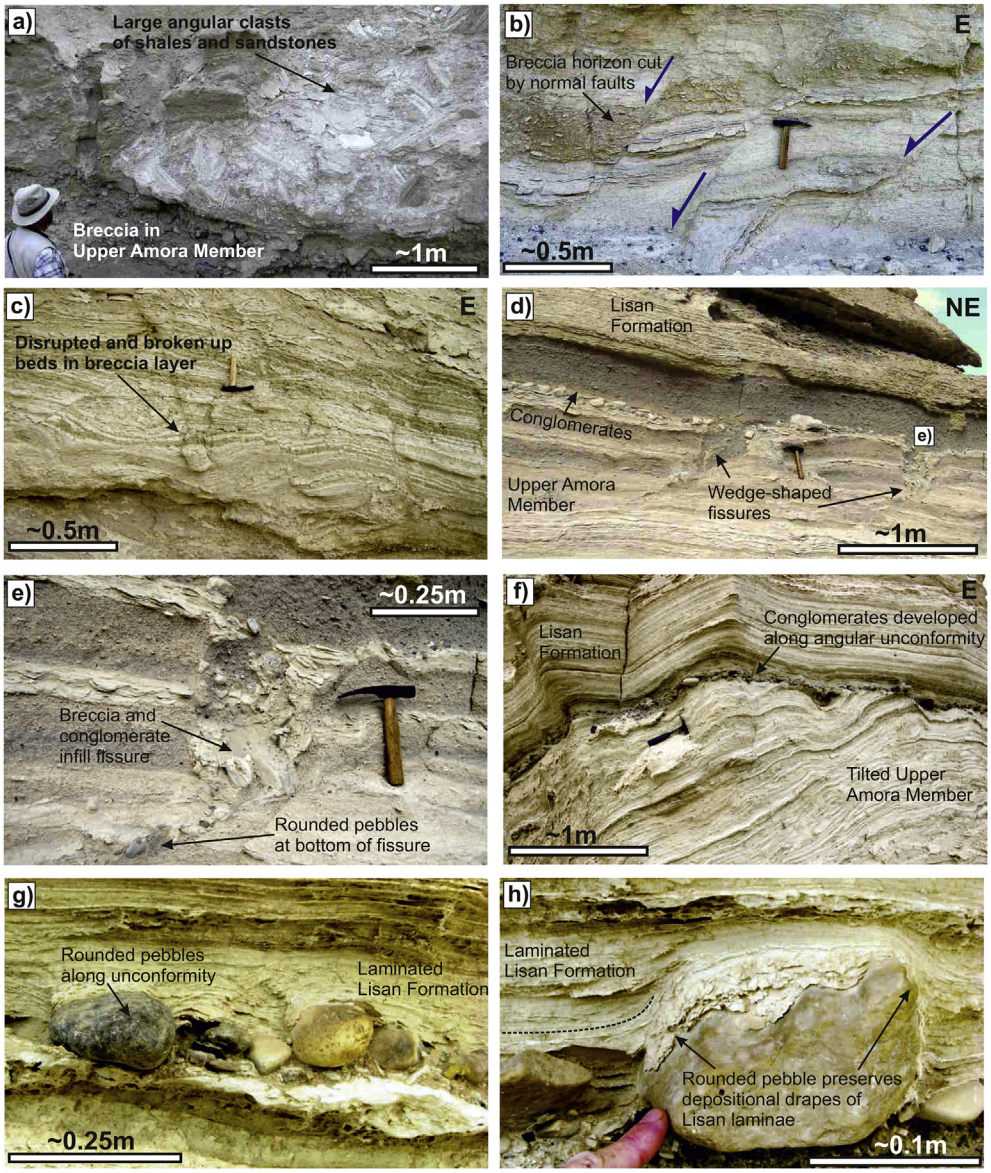

Fig. 7. a, b, c) Photographs of breccias in Upper Amora Member from the NW margin of the Sedom salt wall (N31°06′19.49″; E35°22′01.90″). d, e) Conglomerates defining the base of the Lisan Formation, which is also marked by wedge-shaped fissures infilled by rounded pebbles (N31°03′329″; E35°22′733″). f, g, h) Conglomerates developed along the pronounced angular unconformity between Upper Amora Member and overlying Lisan Formation along the NW Sedom salt wall (N31.10598°; E35.36660°). Rounded pebbles are depositionally draped by laminae of the Lisan Formation. All photographs are viewed with the salt margin towards the East (right) side of the photograph.

infill of the open fissures. Conglomerates are also developed along the actual unconformity surface between Upper Amora Member and overlying Lisan Formation (Fig. 7f). Rounded cobbles comprising carbonates and sandstones up to 10 cm in diameter are draped by overlying laminae of the Lisan Formation (Fig. 7g, h).

3.4. Local syn-sedimentary faults

The Lisan Formation typically comprises an annual varve-like sequence of lacustrine sediments. However, adjacent to the western flank of the Sedom salt wall, syn-sedimentary extensional faults are developed that generate metre scale thickening within the hanging wall sequences reflecting growth geometries (Fig. 8a, b, c). Growth faults are observed in very gently west dipping beds of the Lisan Formation at 215 m and 300 m west of the exposed contact with salt wall. Growth faults typically dip moderately or steeply towards the NE and the diapir contact, and also cut through the unconformity with the underlying Upper Amora Member (Fig. 8a, b). The simplest interpretation is that growth faulting and associated subsidence relate to salt withdrawal to feed the growing salt wall (see discussion 5.1.).

4. Structural record of salt wall growth

4.1. Rotation and upturn of beds towards salt margin

A progressive and sequential upturn of bedding within the Upper Amora Member and Lisan Formation is developed towards the western margin of the Sedom salt wall (Figs. 3 and 9a, b, c). Bedding typically dips variably towards the WSW or WNW in both the Upper Amora Member and Lisan Formation, although is typically steeper in the Upper Amora Member (Fig. 9a). Regional sub horizontal dips are observed in the Upper Amora Member and overlying Lisan Formation at ~1500 m from the diapiric margin (Figs. 3 and 9b).

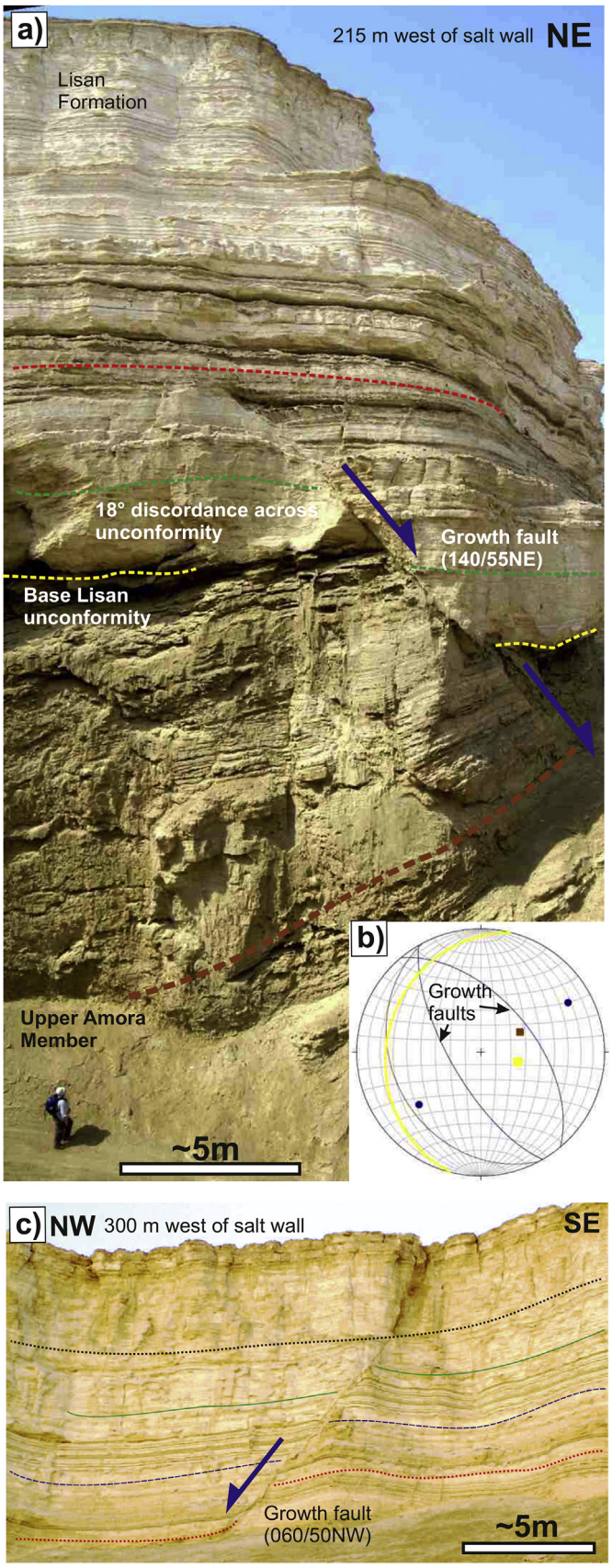

Fig. 8. a) Photograph of growth fault cutting the unconformity at the base of the Lisan Formation at 215 m west of the Sedom salt wall (N31°06′377″; E35°22′600″). On the associated stereonet (b), bedding as shown by great circles and (square) poles in the Upper Amora Member (brown) and Lisan Formation (yellow). Growth faults are also shown as great circles and poles. c) Distinct growth fault developed in the Lisan Formation, with beds picked out by dashed coloured markers (N31°06′338″; E35°22′617″). Photographs are viewed with the salt margin towards the East (right) side of the photograph. (For interpretation of the references to colour in this figure legend, the reader is referred to the web version of this article.)

Westerly-directed dips within the Upper Amora Member start to gradually increase at ~1300 m from the salt, and this is considered to mark the edge of the salt influence at this particular stratigraphic level (Fig. 9b). At 763 m, the westerly-directed dips have increased to 13°, and continue to increase towards the diapiric margin, although the most pronounced upturn occurs within 250 m of the salt (Fig. 9b). The inner-most 100 m of overburden adjacent to the salt is marked by an almost exponential increase in bedding dips, where they have rotated into sub-parallelism with the moderate to steeply dipping diapiric margin (Fig. 9b, c). In summary, the structural record of salt movement is limited to within 1200 m (and typically <500 m) of the diapiric margin.

4.2. Major extensional faults within evaporites of the salt wall

The western margin of the Sedom salt wall is marked by major N–S trending outward dipping normal faults (Zak, 1967, Figs. 3b and 9d; e). These steep faults cut the Lisan Formation, together with the underlying salt and its caprock (Fig. 9f, g), and consistently step up towards the salt wall reflecting the upward movement of the diapir (Zak, 1967; Zak and Freund, 1980) (Fig. 9f, g). The Lisan Formation preserved above the salt wall is also cut by N–S trending extensional faults that locally form grabens, with the Lisan Formation forming gentle synclines within the graben that are possibly caused by salt dissolution and collapse.

4.3. Shearing within overburden sediments

On the SW flank of the Sedom salt wall, extensional shears and faults are developed in the Upper Amora Member within 100 m of the contact with the salt wall (Fig. 9h). These are typically NW–SE trending and dip steeply towards the SW. They deform moderately west-dipping upturned bedding, with an overall extensional top-down-to-the SW sense of displacement (i.e. bottom up towards the NE). These shears are orientated parallel to the steep flank of the salt wall, and are interpreted to reflect the upward movement of salt.

5. Discussion

5.1. What is the geometry and extent of bedding upturn adjacent to a salt margin?

Areas of upturned bedding adjacent to the flanks of salt diapirs and walls have previously been termed ‘drag zones’ (e.g. Alsop et al., 2000), ‘drag folds’ or ‘flap folds’ (e.g. Schultz-Ela, 2003) or ‘drape folds’ (e.g. Giles and Rowan, 2012) (Fig. 1b). They have been studied at outcrop (e.g. Alsop et al., 2000; Rowan et al., 2003; Giles and Rowan, 2012; Hearon et al., 2015a, b), and in seismic sections (e.g. Alsop et al., 1995; Davison et al., 2000a, b; Hearon et al., 2014). In addition, they have been physically modelled (e.g. Alsop, 1996) and numerically simulated (e.g. Schultz-Ela, 2003).

5.1.1. Geometry of bedding upturn

Recognizing that dry sand was too strong to simulate folding and upturn in weak sediments, Alsop (1996) ran experiments using polymer (representing salt) and low-friction glass beads to

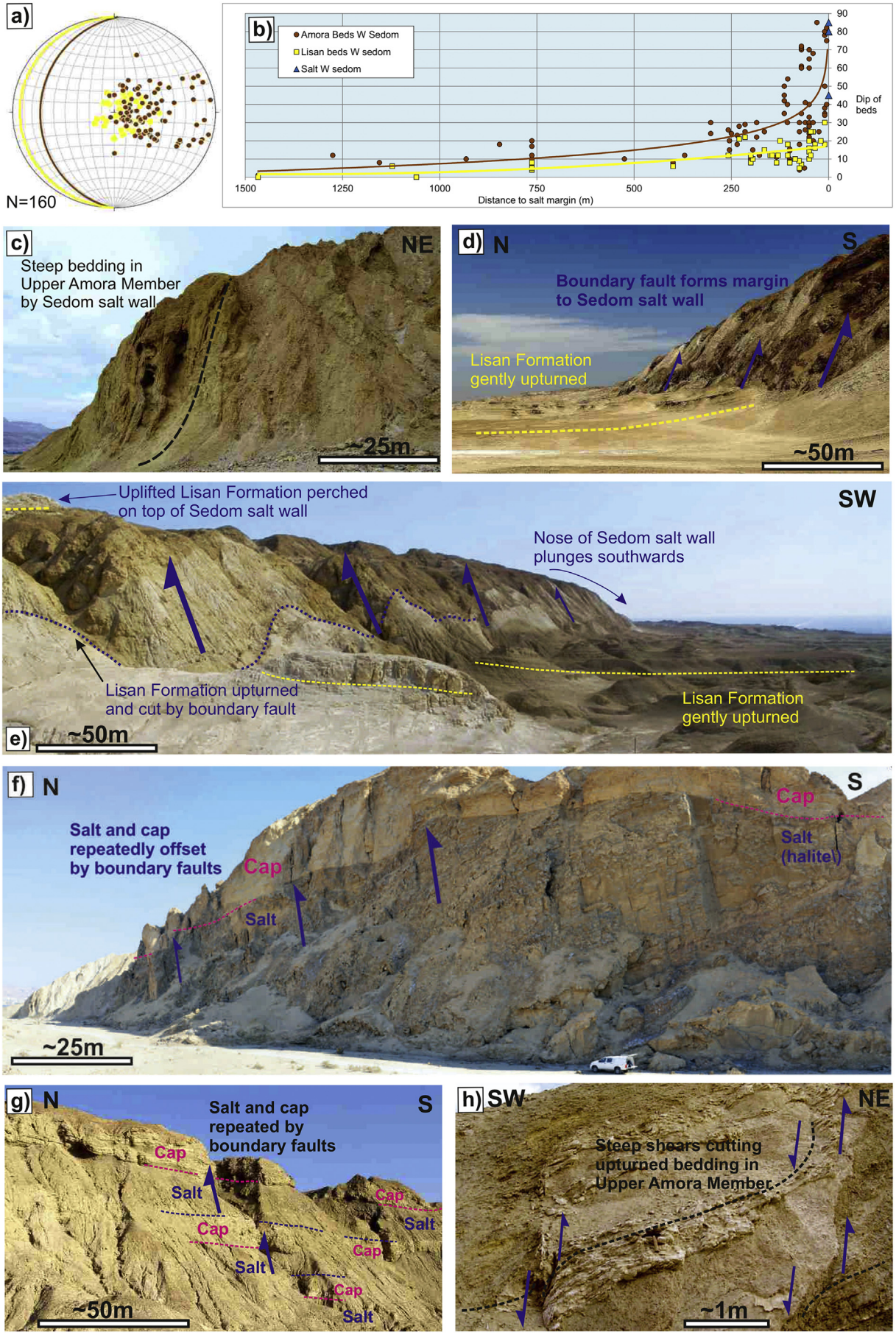

Fig. 9. a) Stereonet of poles to bedding (N = 160) and mean great circles collected from the Upper Amora Member (brown) and overlying Lisan Formation (yellow) that forms the overburden along the western margin of the Sedom salt wall. b) Graph of distance from the western margin of the Sedom salt wall compared to angle of bedding dip (towards the west) within the Upper Amora Member (brown) and Lisan Formation (yellow) (N = 118) Best-fit curves are provided for guidance only. c) Steeply dipping Upper Amora Member adjacent to the NW flank of the Sedom salt wall (N31°07′07.16″; E35°22′26.36″). Photographs d) (N 31°05′24.13″; E35°22′50.41″) and e) (N31°04′33.69″; E35°22′50.90″) showing steeply dipping boundary faults forming the SW margin of the Sedom salt wall, with Lisan Formation cut and carried upwards on the roof of the diapir. The contact between salt and overlying caprock is repeatedly cut by boundary faults that carry the salt upwards in f) NW Sedom salt wall (N31°07′55.16″; E35°22′30.12″) and, g) SW Sedom salt wall (N31°06′52.03″; E35°22′35.09″). h) Steep extensional shears that cut upturned bedding in the Upper Amora Member along the SW flank of the Sedom salt wall (N31°07′04.54″; E35°22′27.89″). (For interpretation of the references to colour in this figure legend, the reader is referred to the web version of this article.)

simulate passive downbuilding of relatively weak overburden around a salt stock. The amount of overburden upturn systematically diminished up the diapiric flanks, as the rate of diapiric growth progressively reduced. The observation that some layers become too long to be restored by simple back-rotation to the horizontal (e.g. Alsop, 1996, Fig. 12a) suggests that stretching and attenuation of these layers had accompanied rotation towards steeper attitudes. Models also display a component of onlap, where younger beds were deposited directly onto older upturned beds, rather than against the diapiric flank itself (Alsop, 1996, p.237).

The numerical modelling of Schultz-Ela (2003, p.761) suggests that salt rising through an overburden of normal strength develops a narrow (100 m wide) zone of upturn that extends to depths of just 200 m below the surface (Schultz-Ela, 2003, p.761). In addition, this work also suggests that upturn of bedding can only occur where sediments have been deposited above the salt and subsequently rotated during its continued rise (Schultz-Ela, 2003). Hudec and Jackson (2011, p.73) noted that "beds adjacent to salt are only upturned if they are originally above the diapir". The observation in this study that growth faults in the Lisan Formation (see section 3.4) were later tilted to the west as the salt wall continued to grow, suggests that portions of the withdrawal basin were subsequently upturned by ongoing salt rise. The implication is that upturn may not be restricted to sediments deposited directly above the diapir, but could also develop at distances of up to 300 m from the flanks of the salt wall.

In the drape fold model of Rowan et al. (2003) and Giles and Rowan (2012), thinner beds are deposited over the bathymetric expression of the underlying salt. Beds are therefore typically inclined and 'draped' away from the crest of the salt structure during their deposition (Figs. 1b and 10a). As subsidence continues around the salt, then bedding dips are enhanced to create drape folds. The amount of overburden upturn in general exponentially increases towards the salt, suggesting an overall power-law relationship associated with deformation of weak overburden (e.g. Alsop et al., 1995, p.9; Alsop et al., 2015, p. 101). Analysis of overburden around the Sedom salt wall shows that the older Upper Amora Member beds have undergone more upturn compared to the overlying Lisan Formation (Figs. 3, 5g and 9 b, c, 10a, b). This is interpreted to reflect greater onlap of the older beds over the diapiric crest, whereas younger beds did not extend as far onto the salt diapir and where therefore rotated less (e.g. Schultz-Ela, 2003; Hudec and Jackson, 2011, p.73).

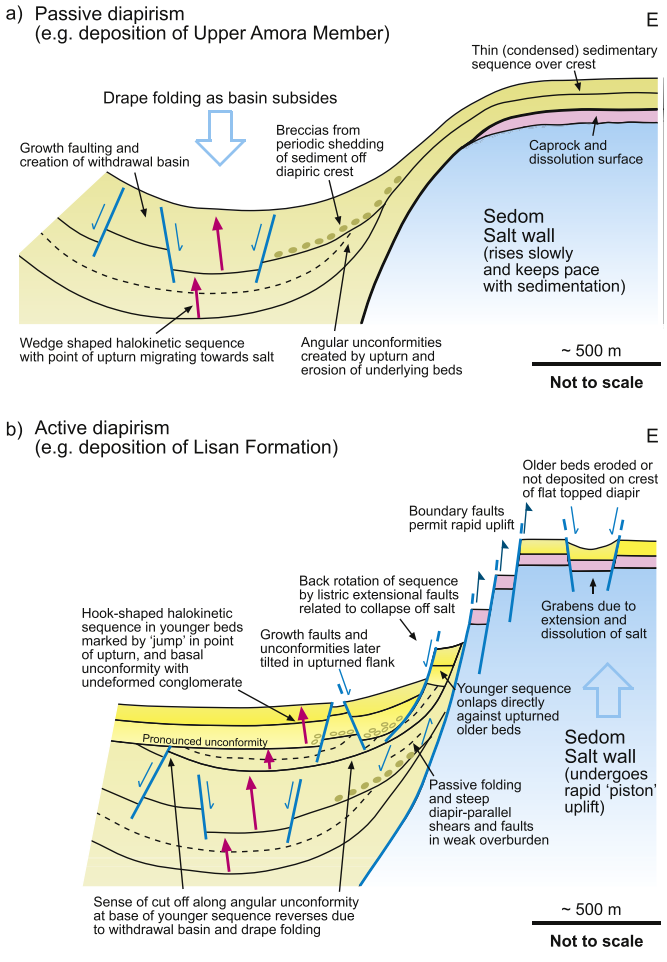

Fig. 10. Schematic cartoons summarising the main features of a) passive diapirism and b) active diapirism during evolution of the Sedom salt wall.

5.1.2. *Extent of bedding upturn*

The recorded widths of upturned bedding around outcrop examples of diapirs vary between 500 m in Nova Scotia (Alsop et al., 2000; Vargas-Meleza et al., 2015) and in the Pyrenees of Spain (Poprawski et al., 2014), up to 700 m wide in La Popa, Mexico (Rowan et al., 2003), and up to 800 m wide in the Flinders Ranges of South Australia (Kernen et al., 2012; Hearon et al., 2015b). It is interesting to note that all of these examples have suffered later regional contraction that may have subsequently affected the geometry of bedding upturn to varying degrees. Seismic analysis of widths of upturn around salt diapirs provides estimates of 1–1.5 km around several North Sea examples, subsequently affected by contraction (Davison et al., 2000b), and up to 680 m around the Auger diapir in the Gulf of Mexico (Hearon et al., 2014). The observed extent of bedding upturn on the NW margin of the Sedom salt wall is up to 1250 m from the exposed salt contact (Fig. 9b), and is therefore wider than typically observed in many diapirs. The greater than normal extent of bedding upturn along the Sedom salt wall may reflect a number of additional factors as discussed below.

5.1.3. *Shape of the salt diapir*

Numerical modelling studies by Schultz-Ela (2003, p.765) suggest that in comparison to cylindrical salt stocks, linear salt walls produce a) wider areas of upturn adjacent to the salt margin, and b) greater subsidence of the overburden adjacent to the salt margin, for equivalent conditions. This difference results from the 3-D radial flow of salt to feed a cylindrical diapir, thereby spreading the area within the source layer from which salt is evacuated, whereas salt walls are fed by a greater component of 2-D (non-radial) salt flow. This concentration of salt flow ultimately results in greater overburden deformation being observed in cross sections across linear salt walls such as exposed at the Sedom diapir.

5.1.4. *Nature of the overburden*

If the overburden is heterogeneous and contains weak layers, such as salt with negligible yield strength, then a significant increase in overburden deformation and folding occurs (e.g. Schultz-Ela, 2003). Notably, the presence of the ~10 m thick Amora Salt Member, combined with other salt beds within both the Lower and Upper Amora Members (Zak, 1967, Table 1), could further reduce the strength of the overburden thereby facilitating greater upturn and deformation adjacent to the Sedom salt wall.

5.1.5. *Increased fluid pressure*

Increasing the overpressure within the overburden encourages and facilitates drape folding (e.g. Schultz-Ela, 2003, p.774). The observation that bedding-parallel gypsum veins are developed in the overburden around the salt wall (Alsop et al., 2015) suggests

that high fluid pressures were indeed locally attained that would further encourage folding.

5.2. What is the geometry and extent of unconformities adjacent to a salt margin?

It has been recognised since the work of Trusheim (1960) that sedimentary sequences around salt diapirs can provide a detailed record of salt movement. This has ultimately led to the concept of halokinetic sequences (Rowan et al., 2003; Giles and Rowan, 2012; Hearon et al., 2014) whereby stratigraphic sequences bound by local unconformities may be linked to adjacent salt movement (Fig. 1b). Unconformities associated with withdrawal basins are marked by beds below unconformities dipping more steeply towards the salt than those above. Conversely, those unconformities linked to upturn of beds adjacent to salt are marked by beds below the unconformity dipping more steeply away from the salt than those above (Fig. 1b). The sense of stratigraphic 'footwall cut-off' along the unconformity surface thereby allows patterns of relative salt movement to be determined (Fig. 10b).

5.2.1. Unconformities – linked to bed downturn and withdrawal basins

Increased diapir-directed dips may relate to salt evacuation to feed the growing Sedom salt wall, leading to subsidence of surrounding sediments and development of 'withdrawal basins'. Physical modelling (Alsop, 1996) has shown that the maximum radii of withdrawal basins is up to 3–4 x larger than the diameter of diapir. In addition, numerical modelling has demonstrated that the location of maximum overburden subsidence associated with the depocentre of syn-diapiric sedimentation sequentially migrates away from the salt wall as it grows (Schultz-Ela, 2003, p.767).

In the Upper Amora Member, the width of downturn and withdrawal basin is greatest in the SW (1500 m) (Fig. 3). In this area, the Upper Amora Member and Lisan Formation locally dip gently (12°) towards the East (Figs. 3 and 6). Some extensional faults operated post tilting of the Upper Amora Member as they cut the tilted unconformity and display Lisan growth geometries (Fig. 8a). The pronounced withdrawal basin within the Upper Amora Member at the SW end of Sedom suggests that the salt wall was fed axially (northwards) along its length (parallel to trend of underlying Sedom Fault), as well as from the deeper basin in the east. The position of this withdrawal basin also suggests that the salt wall has not significantly propagated along strike since deposition of the Upper Amora Member.

InSAR sections and longitudinal profiles from the northern end of the Sedom salt wall display actual subsidence (profiles a, b in Weinberger et al., 2006a). These regions of ongoing subsidence are adjacent to the northern part of the salt wall that is currently undergoing the greatest uplift, and could reflect a modern withdrawal basin with salt evacuating into the growing salt wall. Deflection of drainage by the rising salt wall results in this withdrawal basin being filled by recent alluvial sediments that pond in the depression (Fig. 3b).

5.2.2. Unconformities – linked to bed upturn and drape folds

Giles and Rowan (2012) compare the relative rates of diapir rise and sediment accumulation, and note that these rates control unconformity-bound wedge or hook shaped profiles through halokinetic sequences (HS), created as sediment is shed off the growing salt structure. These halokinetic sequences, each of which "form packages tens of metres in thickness" may be combined to create overall tapered (wedge) and tabular (hook) composite halokinetic sequences (CHS) (Giles and Rowan, 2012, p.8) (Fig. 1b). Where sedimentation rates and downbuilding are greater than diapir rise, they tend to generate broader (up to 1000 m wide) tapered wedge HS (e.g. Hearon et al., 2014) (Fig. 1b). Alternatively, where diapir rise is relatively rapid, then narrower (up to 200 m wide) hook shaped sequences tend to develop (Fig. 1b).

Our data clearly demonstrate that the width of upturn is much greater in the Upper Amora Member when compared to the overlying Lisan Formation (see Fig. 9b). The Upper Amora Member starts to show increased dips at distances of ~1300 m from the salt wall (section 4.1.), and therefore resembles a wedge HS. Conversely, upturn and unconformities within the Lisan Formation initiate at 763 m from the salt, but are largely restricted to within 250 m of the salt (section 4.1., Fig. 9b). They therefore correspond most closely with hook HS. The overall greater width of upturn and halokinetic sequences adjacent to the Sedom salt wall when compared to other diapirs is considered to reflect the linear geometry of the salt wall (as described in section 5.1.3).

The angular discordance across a bounding unconformity surface (whether hook or wedge) varies with distance from the salt contact (see Giles and Rowan, 2012), together with the amount of salt flow and corresponding time 'locked up' across the unconformity surface. Giles and Rowan (2012) note that wedge HS unconformites have angular discordance of <30°, while unconformities associated with hook HS display angular obliquities of <90°. The Upper Amora Member does indeed generally display an angular discordance of <30° with the overlying Lisan Formation. This angle only increases to >30° immediately adjacent (<40 m) to the salt wall where bedding becomes more steeply dipping, and the Lisan Formation onlaps directly on to the upturned Upper Amora Member. We interpret the unconformity between the Upper Amora Member and the overlying Lisan Formation to separate different wedge and hook HS. It therefore represents a composite halokinetic sequence boundary, which Giles and Rowan (2012, their Fig 14b) show as having higher angle discordances, and who also note that lower wedges can indeed "exhibit high angle truncation beneath the composite halokinetic sequence boundary" (Giles and Rowan, 2012, p.9). In summary, generally low-angle and broad unconformity surfaces within the Upper Amora Member match a wedge HS, while the narrower unconformities within the Lisan Formation represent hook HS (Fig. 10a, b). These unconformities show less angular discordance (e.g. section 3.1.1) simply because, as this study demonstrates, each unconformity is separated by much shorter periods of time (~40 ka or less).

Giles and Rowan (2012, p. 22) note that the switch from underlying tapered CHS into overlying tabular CHS, is marked by a pronounced 'jump' in the location of fold hinge zones associated with upturn. These are developed much closer to the salt margin in the overlying tabular CHS. This is clearly observed when comparing upturn in the Upper Amora Member wedge HS that initiates at distances of up to 1250 m in the NW of the Sedom salt wall, with that in the overlying Lisan Formation hook HS that typically occurs at distances of <100 m (Fig. 9b). It should be noted that these models of halokinetic sequences were originally developed for passive diapirs (Giles and Rowan, 2012), and do not take into account that rapid salt rise may be associated with active diapirism. However, Rowan et al. (2003) do recognise that overall passive diapirism actually entails cycles of subordinate active diapirism, where the sedimentary overburden covering the diapiric crest is periodically lifted and shed from the roof of the rising salt (e.g. Hearon et al., 2014, 2015a, b).

Following the general methodology of Waldmann (2002) and Poprawski et al. (2014), the minimum amount of net salt rise may be estimated by measuring angles of obliquity (or the 'taper angle' of Hearon et al., 2014) across dated unconformities (Table 2). Tilting of horizontal beds is assumed to be achieved by the upward movement of salt relative to the overburden. Using this method,

Waldmann (2002) measured angles of tilting at distances of 2 km from the Sedom salt wall and suggested a decrease in the rate of uplift of the salt wall during deposition of the Lisan Formation. Our own estimates are based on angles of tilting at 763 m from the salt and indicate an increase in the rate of salt uplift from 1.37 mm/year during deposition of the Upper Amora Member (167–70 ka) to 2.33 mm/year during deposition of the overlying Lisan Formation (Table 2). We suggest that these differences arise as Waldmann's (2002) estimates were based on angles of tilting at distances of 2 km from the salt wall (rather than 763 m), and as such become increasingly inaccurate due to extrapolation over longer distances. In addition, this technique provides only a crude minimum estimate of salt rise as it takes no account of a) salt dissolution or sediment compaction; b) increased amounts of tilting near the salt contact; c) discrete faulting in the overburden; d) potential modification of cut-off angles by subsequent flexural slip across unconformities (e.g. Hearon et al., 2014). However, given these not insignificant constraints, our estimates do suggest that the rate of salt rise significantly increased at about 70 ka during deposition of the Lisan Formation (Table 2).

5.3. At what depth does upturned bedding develop adjacent to a salt margin?

There has been a long standing debate regarding the depth at which bedding upturn develops adjacent to diapiric flanks (e.g. Johnson and Bredeson, 1971; Alsop et al., 2000; Schultz-Ela, 2003; Rowan et al., 2003; Poprawski et al., 2014; Hearon et al., 2014). During flap folding, sediments are deposited parallel or sub-parallel to the contact with the underlying salt, and rotated shortly afterwards as sediments subside and the salt continues to rise close to the surface (Fig. 1b). Conversely, traditional models had suggested that bedding had been deposited at high angles to the salt margin, and subsequently rotated into parallelism by frictional drag along the salt contact at greater depths, as the diapir penetrated from below. Schultz-Ela (2003, p.777) states that "flap folds form because of the differential movement of sediment and salt, regardless of whether the sediment actually subsides or the salt rises". The advantage of studying a recent and actively growing diapir is that it has not been buried by sediment, and the observed geometries cannot therefore be complicated by the possibility of deeper processes and/or subsequent tectonism.

The exposed unconformity at the base of the Lisan Formation associated with areas of upturn around the Sedom salt wall permits some simple calculations regarding the amount of overburden that may exist at the time of folding. Table 3 provides maximum and minimum estimates of the thickness of the exposed Upper Amora Member sediments that may have been eroded across the angular unconformity at the base of the Lisan Formation. These estimates are based on extrapolating the angular obliquities in bedding dips recorded across the unconformity at different distance intervals from the salt margin. This estimate assumes that a) the upturned beds display a parallel style of folding, such that the orthogonal thickness of beds does not alter during folding, and b) the sediments did not undergo stratigraphic thinning towards the crest of the salt wall to create a sediment wedge shape. If either of these assumptions are incorrect then it is likely that the calculated burial depths are in fact an over estimate. Our trigonometric calculation suggests that a maximum thickness of between 155 m and 295 m of Upper Amora Member may have been removed along the base Lisan unconformity (Table 3). We suggest that total burial could in fact be significantly less than this if, as seems likely, the Upper Amora Member itself was undergoing depositional thinning and slumping off the Sedom salt wall (Alsop et al., 2015) (Fig. 10a), or was undergoing a non-parallel style of folding (see 5.4). The upturned bedding that is observed around the Sedom salt wall must therefore be a product of surficial or very shallow deformation within a few hundred metres of the surface.

5.4. Is deformation concentrated along unconformites adjacent to a salt margin?

5.4.1. A flexural slip fold model

Classical models of drape folding associated with salt rise indicate that flexural slip is concentrated along unconformity surfaces that bound halokinetic sequences (e.g. Rowan et al., 2003). This unconformity-parallel shear is a geometric necessity of the model in order to permit rotation between halokinetic sequences and thereby maintain compatibility between variably-dipping adjacent sequences. The sense of shear along each surface will be top-towards-the diapir, in response to relative upward movement of salt coupled with overall flexural slip between the halokinetic sequences (Rowan et al., 2003, 2012; Giles and Rowan, 2012). It is suggested that deformation is focussed by slip along upturned bedding planes that converge along onlap surfaces associated with angular unconformities (Rowan et al., 2003). Rowan et al. (2003, p. 754) note that "concentration of slip along the unconformities makes them equivalent to faults" and they are interpreted to result in pointed cusps along the salt flank where sheared unconformities intersect with the salt margin (Fig. 1b).

Although a necessity of the model, field evidence to directly support shearing along exposed unconformities is limited, with recent outcrop work by Ringenbach et al. (2013), Callot et al. (2014) Poprawski et al. (2014) and Li et al. (2014) all making no mention of deformation along well-exposed unconformities. However, Hearon et al. (2015b) have recently recorded slip on unconformities around diapirs in the Flinders Range of South Australia while Rowan et al. (2003, p. 738) note 20 cm thick brittle shear zones comprising brecciated lithologies in a carbonate cement along unconformity surfaces around the El Papalote diapir in Mexico. The sense of shear results in beds above the unconformity undergoing relative translation towards the diapir. Bedding-parallel slip in upturned sequences around salt diapirs has also previously been documented in both field studies (e.g. Alsop et al., 2000) and from drill cores (e.g.

Table 3
Estimates of thickness of Upper Amora Member removed by erosion across the base Lisan Formation unconformity at different distances from the exposed salt contact. Estimates are based on angle of obliquity across the unconformity surface and do not take thinning of the sedimentary wedge into account. The minimum estimate is based on extrapolating the outer (lower dip) value in each case, while the maximum estimate is based on extrapolating the inner (higher dip) value. Minimum and maximum values are inserted in parenthesis. See Fig. 9b for data.

	Distance from exposed salt contact (m)					
	750–215 m	215–75 m	75–40 m	40–10 m	10–0 m	Total
Minimum estimate	65.2 m (7°) Total = 65.2 m	43.3 m (18°) Total = 108.5 m	16.6 m (29°) Total = 125.1 m	20.8 m (44°) Total = 145.9 m	9.4 m (70°) Total = 155.3 m	**155.3 m**
Maximum estimate	165.3 m (18°) Total = 165.3 m	67.9 m (29°) Total = 233.2 m	24.3 m (44°) Total = 257.5 m	28.2 m (70°) Total = 285.7 m	9.4 m (70°) Total = 295.1 m	**295.1 m**

Davison et al., 2000a), although as noted by Rowan et al. (2003) the contribution of later regional shortening is unknown in each case.

Unconformities around the Sedom salt wall are locally marked by conglomerates containing pebbles within a fine silt matrix that would potentially act as ideal markers for any deformation that had subsequently taken place (Fig. 7f, g, h). The pebbles are interpreted as being originally incorporated within channels of the Amora Formation. We suggest that salt induced tilting ultimately resulted in erosion and winnowing of finer sands and silts within the Amora Formation, with the pebbles being concentrated as a lag deposit along the angular unconformity. There is no available source for these pebbles within the diapir itself, and the most likely source is the Cretaceous exposed in the footwall of the rift margin fault 2 km to the west (Fig. 2b). The roundness of the clasts suggests that they are relatively far-travelled and/or reworked several times. The pebbles themselves are subsequently draped by fine laminae of the Lisan Formation, and there is no evidence for rotation or rolling of clasts associated with subsequent deformation being concentrated along this boundary i.e. laminae between pebbles retain pristine relationships to one another and the clasts (Fig. 7g, h).

Thus, pebbles maintain pristine relationships with draped silt laminae, which also contain well preserved cross laminations. The conclusion that can be drawn is that despite underlying beds having been rotated to dips of 17°W and the unconformity itself marked by an obliquity of 7°, there was no appreciable concentration of shear along this boundary and alternative models for accommodating deformation of halokinetic wedges therefore need to be considered.

5.4.2. A passive fold model

A pre-requisite for flexural slip is the deforming rocks or sediment "are layered or have a strong mechanical anisotropy" (Fossen, 2010, p.232). We suggest that the unlithified shales and sands of the Upper Amora Member are unlikely to possess a strong mechanical anisotropy at the time of folding, and a passive fold model, where "layering exerts no mechanical influence on the folding" (Fossen, 2010, p.229) is therefore more likely in this case. Rather than deformation being concentrated along unconformities, we therefore propose that diapir-parallel slip and shear could be focussed throughout weaker shale and mud units, Diapir-parallel shears cutting through competent units are not thought to develop (e.g. Rowan et al., 2003) because the shear strength of salt is so much weaker than the overburden sediment, resulting in most of the shear along the salt-sediment interface being concentrated within the salt itself (e.g. Schultz-Ela, 2003, p.760). Hearon et al., 2014 (p.69) state that owing to limitations of seismic data that they could not rule out "a component of diapir-parallel faulting or shearing, especially in less competent shales". However, diapir-parallel steep extensional faults that consistently display relative uplift towards the diapiric margin are preserved in examples from Nova Scotia (e.g. Alsop et al., 2000). Similar diapir parallel shear are also preserved within upturned shales of the Upper Amora Member along the SW flank of Sedom salt wall (Figs. 9h and 10b). These shears display a footwall up to the NE sense of movement i.e. consistent with salt intrusion to the NE, but opposite to the kinematics expected for flexural slip. In order to account for the observed shears within beds, we suggest that a passive folding mechanism, whereby deformation is distributed throughout weaker beds as they undergo bending and 'forced folding' linked to salt rise, may be more appropriate in this case. A lack of flexural slip also means that obliquities across unconformities have not been modified (see Giles and Rowan, 2012; Hearon et al., 2014) and pristine cut-off angles are preserved.

5.5. How is diapiric uplift achieved without widespread deformation adjacent to a salt margin?

Although the Sedom salt wall has lifted the overlying Lisan Formation more than 75 m above its regional elevation in the past 15.5 ka (Weinberger et al., 2006a, 2007), there remains a distinct lack of widespread deformation in these sediments. This apparent anomaly may be explained by a number of factors.

5.5.1. The role of active diapirism

It has been proposed previously that passive diapirism typically generates pronounced areas of upturn adjacent to salt margins, (e.g. Davison et al., 2000a, b), whereas active diapirism could form more localised areas of deformation associated with faulting (e.g. Schultz-Ela, 1993) (Fig. 1a, b, 10a, b). Weinberger (1992) and Weinberger et al. (2006a) have calculated the minimum thickness of overburden required for density inversion to develop around the Sedom salt wall as between 550 m and 1650 m, with a likely value of ~1000 m for a mixed shale and sand overburden (as observed in the Amora Formation). Drilling has shown that the Sedom salt horizon is covered by an overburden of 1900 m and 3700 m to the west and east of the Sedom salt wall respectively, and that the conditions for positive salt buoyancy are therefore met (Weinberger et al., 2006a). Further to the east in the centre of the basin, the Sedom salt is overlain by 5500 m of overburden, which imparts a buoyancy force that would allow the salt to rise to 384 m above the level of the Dead Sea (Weinberger et al., 2006a, p.48). The salt currently reaches a height of 250 m above the Dead Sea level, suggesting that a potential buoyancy-driven rise of a further ~130 m is theoretically possible, although it is likely that collapse of salt would initiate before that height was actually attained (see Davison et al., 1996b). In summary, the conditions for halokinetic active diapirism (Hudec and Jackson, 2011, p.74) are clearly fulfilled by the Sedom salt wall, with active uplift of the salt currently continuing at rates of between 5 and 8 mm/year (Weinberger et al., 2006b) and potentially up to 11 mm/year (Zucker, 2014).

5.5.2. The role of diapiric roof geometries

Modelling studies by Schultz-Ela et al. (1993) have demonstrated that active diapirism is most readily achieved by a 'flat topped' rectangular shaped diapir rather than those with pointed or arched roofs. In addition, diapir height should be >66% of the thickness of the adjacent overburden for substantial active diapirism to occur. Clearly, the 3–4 km height of the emergent Sedom salt wall above the source layer (Weinberger et al., 2006a) is significantly greater than this minimum threshold of overburden thickness. In addition, dissolution of the top of the Sedom salt wall has resulted in the development of a relatively flat surface marked by a 'salt mirror' dissolution plane and overlain by a 40 m thick caprock (Zak, 1967) (Fig. 10b). A consequence of this 'flat roofed' geometry is that compared to more typical arched roof shapes, there is less necessity for tilting and shedding of overlying sediments, resulting in the observed lack of breccia horizons in the Lisan Formation linked to salt uplift. The flat topped diapiric crest could also result in very little depositional dip or 'tapering' of Lisan sediment wedges above the salt wall. This lack of tapering may limit the extent of sediment over the salt wall, thereby also resulting in less sediment being deformed. Thus, the 'height' of the Sedom salt wall, coupled with its 'flat topped' geometry, makes it particularly suitable for active diapirism and limited extent of deformation in surrounding overburden.

5.5.3. The role of boundary faults

Existing models suggest that most of the shear along the salt-sediment interface should be concentrated within the salt, due to

its relative weakness compared to sediments (e.g. Schultz-Ela, 2003, p.760). However, if absolute rates of salt rise and sedimentation are rapid, then high strain rates may cause the flank of the salt diapir to behave as a brittle fault (Rowan et al., 2003, p.749) (Fig. 1a). Indeed, we observe 'synthetic' normal faults (Schultz-Ela et al., 1993; Hudec and Jackson, 2011) on each flank of the Sedom salt wall, as the salt rises at average rates of 5 mm/year over the past 15.5 ka (e.g. Weinberger et al., 2006a). The boundary faults marking the edge of the Sedom salt wall are recently active as they cut the salt and its overlying caprock, the latest phase of which developed during dissolution at 14–11 ka (Zak, 1967, Weinberger et al., 2006a, Fig. 3b). In addition, the faults correspond to marked surface uplift on InSAR maps (e.g. profiles, j, k in Weinberger et al., 2006b). In such an active intrusion model, there is no necessity for marked upturn of beds around salt diapirs as deformation is accommodated along the bounding faults rather than distributed within the salt or adjacent overburden (e.g. Hearon et al., 2014, p.71) (Fig. 10b).

Sequentially rotated unconformities developed just 70 m from the SW margin of the Sedom salt wall, suggest that the Lisan Formation was back-tilted along listric faults to dip towards the salt, with unconformably overlying Lisan beds dipping progressively more gently towards the diapir (Fig. 6f). Such back-rotation of beds and unconformities along listric faults can only be achieved by down throw of the hanging wall rather than uplift of the footwall, and are therefore considered to relate to progressive collapse of overburden off the rapidly rising salt diapir. Rotation of overburden blocks along listric faults results in beds dipping variably towards the diapir, thereby disrupting the sealing potential of a salt flank to fluids and hydrocarbons.

In summary, as originally recognised by Zak and Freund (1980), the uplift of the Sedom salt wall is largely achieved through the boundary faults and shear zones that form the flanks to the diapir (Fig. 10b). We suggest that if earlier dissolution created a horizontal and relatively 'flat top' to the diapir, then it is more likely that sediments subsequently deposited over the crest will simply be carried upwards, rather than being rotated, tilted and shed off the crest. Boundary faults will cut off any draped sediment overlying the salt meaning that it is then carried passively upwards with a rising, flat-topped 'piston' of salt (Fig. 10b). Local collapse of overburden off the rising salt piston may be achieved along listric extensional faults. Thus, uplift does not necessarily equate to wholesale tilting and deformation of overlying sediments if salt rise is achieved across steep bounding faults.

5.6. What are the rates and durations of diapiric cycles recorded adjacent to a salt margin?

Hearon et al. (2014, p.70) suggest time scales ranging from approximately 50 ka to 1 Ma for each composite halokinetic sequence (CHS) that develops around a deep water diapir in the Upper Miocene to Pleistocene of the northern Gulf of Mexico. When compared to the broader tapered CHS, Hearon et al. (2014) found that the tabular CHS typically give shorter time intervals of 130–200 ka. The shallow water La Popa diapir of northern Mexico that developed in the late Cretaceous generates CHS that formed over much longer intervals, which Giles and Rowan (2012, p.8) describe as "ranging from several hundred thousand years to several millions of years" while Hearon et al. (2014, p.70) quote timescales of 1–10 Ma for these sequences. In each of these cases, the CHS intervals broadly match rates of sea level variation that are considered to be one of the major controlling factors in their development (Hearon et al., 2014, p.70).

While the broad timescales noted above provide estimates for the duration of CHS, individual hook and wedge HS within such sequences have not been dated. Adjacent to the Sedom salt wall, the Upper Amora Member displays a pronounced unconformity dated at 167 ka (Waldmann et al., 2007, 2009), which provides an estimate of 97 ka for the duration of a wedge halokinetic sequence (HS) at the top of this member (dated at 70 ka). As a 116 ka marker bed (Waldmann et al., 2007) displays a similar orientation to the underlying 167 ka unconformity surface (Fig. 4b), it is likely that the tilting event actually occurred over a shorter (46 ka) timescale between 116 and 70 ka. Within the overlying Lisan Formation, dating of individual unconformities that bound a hook halokinetic sequence to 70 and 30 ka provides an estimate of just 40 ka for this hook HS (Table 2, Figs. 4 and 5). Furthermore, isotopic dating indicates that cycles of passive and active diapirism along the Sedom salt wall may last for as little as < 30 ka, with actual switches between styles operating on timescales significantly less than this (Fig. 11, see section 6 below). Although we are dealing with individual halokinetic sequences, the time spans calculated for wedge HS (97 ka), hook HS (40 ka) and switches in active and passive diapirism (30ka) along the Sedom salt wall are a fraction of the 50 ka to1 Ma estimated for CHS around Upper Miocene to Pleistocene diapirs in deep water settings (Hearon et al., 2014). In addition, they are 1–2 orders of magnitude less than the suggested 1–10 Ma duration for CHS adjacent to shallow water diapirs in the late Cretaceous (Hearon et al., 2014; Giles and Rowan, 2012). Despite the more rapid development of halokinetic sequences around the Sedom salt wall, the geometries and widths of upturn of the overburden appear to be similar (if not even wider) than these other examples. Fluctuations in the water level of tens of metres in Lake Lisan have previously been considered to have a significant effect on the behaviour of the Sedom salt wall (Weinberger et al., 2006a, b). We therefore suggest that the shorter duration of HS around the Sedom salt wall, together with the dramatic switches in cycles of active and passive diapirism reflects the more rapid fluctuations in water levels and sedimentation in a lacustrine and subaerial environment, compared to deep water settings. In addition, the inherently greater resolution provided by outcrop studies of recent and ongoing diapirism, when compared to older structures preserved in the geological record, or those imaged through seismic analysis alone, may also help create a more refined template for diapirism as witnessed along the Sedom salt wall.

6. Model of transitions from passive to active diapirism within the Sedom salt wall

We now provide an evolutionary model for the development of active and passive diapirism along the Sedom salt wall, with some general time constraints provided by stratigraphic relationships and isotopic dates.

6.1. Sedom salt wall from 420 ka to 70 ka

Parts of the Sedom salt wall were exposed at 420 ka when an extrusive salt sheet flowed towards the NE and the depocentre of the basin (see Alsop et al., 2015 for details). From 340 to 80 ka, the salt wall then became submerged during deposition of the Upper Amora Member (Alsop et al., 2015) (Fig. 11). The Upper Amora Member comprises sands, silts, gravels, and conglomerates that are considered to have been deposited relatively rapidly. Although the Upper Amora Member is only preserved above the central and northern portions of the Sedom salt wall where it has not been significantly tilted, it is thought to have originally covered the whole diapir as drape folds and unconformities are developed along the entire western flank of the salt wall (Fig. 10a). In addition, breccia horizons formed when sediment was shed off the rising salt diapir are also observed along the western margin. The Upper Amora Member is currently only preserved in the central segment

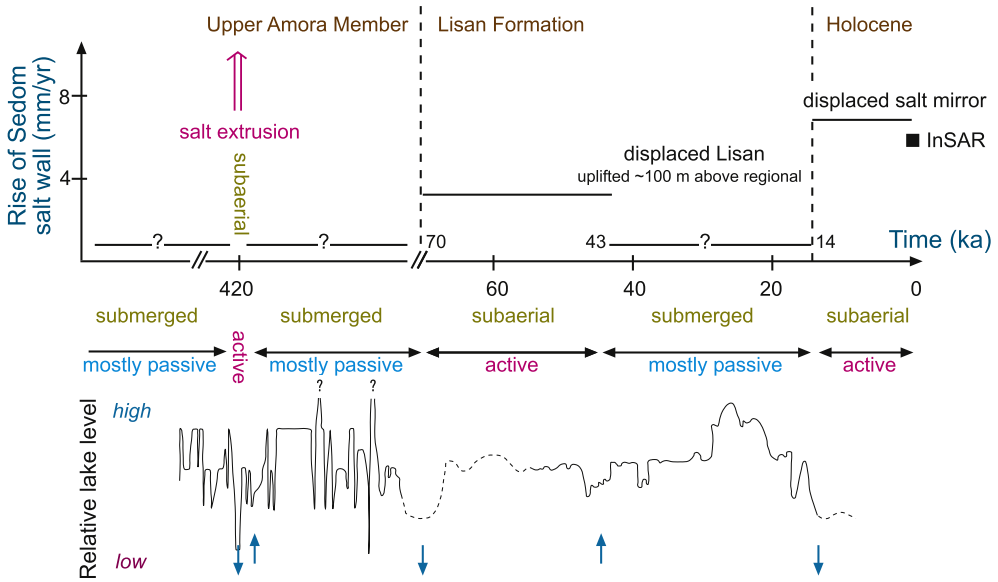

Fig. 11. Diagram summarising the timing, rates of salt rise and lake level fluctuations for passive and active diapiric cycles along the Sedom salt wall. The relative lake level curves are compiled from Torfstein et al. (2009) and Waldmann et al. (2009) for the Upper Amora Member and Bartov et al. (2002) for the Lisan Formation.

as a) it may have been originally thicker there, as it was deposited above a subsiding vent that fed the earlier salt flow, b) more uplift in the North and South of the salt wall may have resulted in greater erosion of overlying sediments.

In summary, the Sedom salt wall was undergoing a prolonged phase of passive diapirism during this period marked by rotated unconformities and halokinetic sequences, interspersed with shorter intervals of active diapirism associated with salt extrusion (at 420 ka) and breccia horizons reflecting shedding of sediments off the rising diapir (Fig. 10a).

6.2. Sedom salt wall from 70 ka to 43 ka

Lisan Formation was not deposited over the crest of the Sedom salt wall between 70 and 43 ka, indicating that it was subaerially exposed at this time (Weinberger et al., 2006a) (Fig. 11). Beach and shoreline facies are however developed within parts of the Lisan Formation immediately west of the salt wall, suggesting that the diapir may have formed a 'Sedom Island' or peninsular within the hypersaline Lake Lisan (Weinberger et al., 2007). It is important to note that this period of subaerial exposure coincides with increased angles of tilting around the western margins of the salt wall, inferred to represent more rapid salt rise, and may also coincide with the removal of the Upper Amora Member from large parts of the salt wall (Fig. 10b). Minimum estimates of salt rise between 70 and 30 ka are 93 m at rates of 2.33 mm/year (Table 3). The Lisan Formation onlaps directly onto the upturned Upper Amora Member (rather than underlying salt) in NW Sedom (Fig. 5g). The Lisan Formation is marked by hook-shaped halokinetic sequences, in contrast to the underlying Upper Amora Member which displays wedge-shaped profiles (Figs. 1b and 10b). In summary, the Sedom salt wall was undergoing a prolonged phase of active diapirism during this period, which is associated with subaerial exposure of the crest, and development of hook-shaped halokinetic sequences.

6.3. Sedom salt wall from 43 ka to 14 ka

The base of the Lisan Formation exposed on top of the Sedom salt wall has been dated as 43 ka, and rests with an angular unconformity directly on the tilted Bnot Lot shales Member (Fig. 11, Table 1). The recognition that the Lisan Formation was deposited over the crest of the diapir indicates that it was inundated and submerged by Lake Lisan from 43 ka to 14 ka. The increase in NaCl within the Lisan Formation at 43 ka may reflect large-scale dissolution of the Sedom salt wall at this time (Weinberger et al., 2006a). Thickening of the Lisan Formation within downfaulted graben on the crest of the Sedom salt wall may also reflect dissolution and collapse of the underlying salt (Fig. 10b). Rotated unconformities and growth faulting in the Lisan Formation on the flanks of the Sedom salt wall (Figs. 4d, 5a, b, and 8a, c) indicate that it is undergoing mostly passive diapiric growth at this time.

6.4. Sedom salt wall from 14 ka to present

At 14 ka, the level of Lake Lisan dropped and the Sedom salt wall once again became subaerial (Fig. 11). Weinberger et al. (2006a, p.48) note that "a substantial topographic rise (along the Sedom salt wall) took place mainly since the early Holocene" They partly attribute this to a marked fall in the water level of Lake Lisan at this time, which had previously dissolved the rising salt and thereby prevented it from forming a pronounced feature. The last phase of dissolution to create the most recent cap rock occurred at 14–11 ka (Weinberger et al., 2006a), with the horizontal base to this cap rock (or 'salt mirror') indicating little or no tilting since this time, despite significant uplift (Fig. 10b). The stratigraphic top of the Lisan Formation is dated at 15.5 ka and has been carried 75 m above regional elevations on the crest of the salt wall (Weinberger et al., 2007). This latest extrusive phase is marked by a dramatic increase in uplift rates, as frequently observed in other diapirs that display accelerated strain rates that are 3–4 orders of magnitude greater than salt flow at depth (Talbot and Jackson, 1987). The thickness of the 'perched' Lisan Formation sitting on top of the rising salt wall is < 40 m, and therefore within the broadly suggested limits (50 m) that active diapirs may carry upwards (Davison et al., 1996a).

The most rapid uplift recorded by InSAR is in the area immediately to the north of the central pinched section of the salt wall, where the salt is overlain by the Upper Amora Member and is bound to the west by a marginal fault (Zak, 1967). These areas of

uplift notably coincide with the thickest deposits of Upper Amora Member that sit above the salt, and correspond to the interpreted former vent that fed an extrusive salt sheet (Alsop et al., 2015). The Upper Amora Member does not appear to be cut by marginal faults everywhere, and in some cases appears to be in stratigraphic continuity and simply 'drapes' over the salt (Fig. 3). These areas may be considered the less evolved portions of the Sedom salt wall.

The top of the Lisan Formation has been uplifted to 75 m above regional, suggesting mean rates of the order of ~5 mm/year. The additional uplift, compared to estimates based on angles of overburden tilt (Table 2), can be accounted for by displacement on discrete faults that bound the diapir (Fig. 10b). The observation that similar amounts of uplift are recorded from the past 15.5 ka (75 m) or 11–14 ka (80 m), when compared to older 43 ka horizons (~100 m uplift), suggests that most of the uplift has taken place during the Holocene. This is supported by the observation that boundary faults not only cut the Lisan Formation on the Sedom salt wall (and were therefore active at post-43 ka), but also the caprock overlying salt that developed as recently as 11–14 ka (Fig. 9f, g, 10b). The acceleration in salt wall uplift demonstrated by InSAR, when compared to averaged rates, reflects salt breakout at the surface.

In summary, removal of the Upper Amora Member that formed a roof to much of the Sedom salt wall occurred at between 70 and 43 ka (Weinberger et al., 2007), and this may then have facilitated more rapid and active rise of the salt diapir (Fig. 11). Largely passive growth during deposition of the Upper Amora Member (Fig. 10a) is followed by more active diapirism in Lisan times when salt was emergent and rising at ~5 mm per year (Fig. 10b). The switch from wedge (Upper Amora Member) to hook (Lisan Formation) halokinetic sequences marks increasing diapiric rise, ultimately resulting in the currently observed phase of active diapirism where salt has broken out at the surface.

7. Conclusions

The Sedom salt wall displays differing relationships with overburden along its 10 km length and has the distinct advantage over circular salt stocks of potentially preserving diapiric processes such as withdrawal basins, upturn, draping and marginal faults at different stages of evolution. The northern and southern ends of the intrusion display the most evolved scenario marked by steep boundary faults and pronounced withdrawal basins, suggesting that some salt flowed axially into the salt wall, whilst the central portion is the least evolved and still preserves sedimentary cover (Upper Amora Member) that is gently draped over the crest of the salt wall. The Sedom salt wall therefore presents an opportunity to study deformation and drape folding associated with passive diapirism, together with boundary faults and uplift patterns marking active diapirism. These processes have been 'caught in the act' at varying stages of development, and lead us to the conclusions listed below.

a) Upturned bedding within overburden extends for up to 1250 m from the Sedom salt wall, with the most pronounced dips (typically > 40°) reserved for the inner 100 m. These broad areas of upturn are wider than typically recorded around many diapirs and are considered to be enhanced by the elongate shape of the salt wall (which essentially constrains salt influx into 2-D flow), the heterogeneous and weak overburden which contains evaporites, and potentially high fluid pressures around the diapir as demonstrated by gypsum veining.
b) Angular unconformities within the overburden may relate to underlying beds displaying either i) increased dips towards the salt, reflecting the outer margins of withdrawal basins and extending for up to 1500 m from the diapir, or ii) increased dips away from the salt reflecting upturned bedding and drape folding for distances of up to 1250 m from the diapir. The older Upper Amora Member shows a broad wedge shaped halokinetic sequence, while the overlying Lisan Formation displays a narrow hook-shaped profile. The obliquity across the angular unconformity at the base of the Lisan Formation therefore increases towards the salt margin. These difference are considered to reflect i) greater rates of sedimentation and generally passive diapirism during deposition of the Upper Amora Member, ii) greater rates of salt rise and more active diapirism during deposition of the Lisan Formation.
c) Contrary to many studies of salt diapirs, the overburden around the Sedom salt wall has not suffered later contractional deformation and has never been deeply buried. The Lisan Formation is overlain by just a few metres of overburden, and together with the unconformable contact with the underlying Upper Amora Member is upturned towards the Sedom salt wall. These directly observed areas of upturned bedding therefore preserve pristine relationships created at shallow (less than a few hundred metres) depths. Sedimentary breccias and growth faults within the overburden attest to the salt-sediment interaction and confirm a surficial drape fold model for upturned bedding around this diapir.
d) Unconformity surfaces exhibit pristine sedimentary relationships and we find no evidence of flexural slip deformation being concentrated along rotated unconformities adjacent to the salt wall. We do however observe diapir-parallel shear within incompetent units and suggest that in this case, a passive folding mechanism, where deformation is concentrated into weaker lithologies during bending associated with 'forced folding', may be a more appropriate mechanism to accommodate diapir-related uplift.
e) The Lisan Formation deposited on top of the Sedom salt wall at 43 ka was carried upwards to 100 m above its regional elevation at rates of 5 mm/year. This uplift was largely achieved via movement on the bounding marginal faults that define most of the western flank of the salt wall. If these boundary faults allow the flat-topped salt wall to rise like a piston (during active intrusion) then they will cut off and laterally truncate any sediments that are draped across them. There is then no necessity for these detached sediments to rotate (as in classic drape fold models) as they will be carried rapidly upwards on the flat roof of the actively rising salt wall. In some cases collapse of overburden along listric faults results in back-rotation of overburden blocks resulting in anomalous dips toward the salt.
f) The switch from passive to active diapirism along the Sedom salt wall, which occurred over at least 3 separate cycles from 420 ka to present, is marked by more rapid rates of uplift perhaps facilitated by surface break out of salt, lowering of lake levels to reduce dissolution of salt, erosion of Upper Amora Member overburden from above the salt, and weakening of overburden by local extensional faulting. Our field observations, coupled with a refined stratigraphic template supported by isotopic dating permits a more detailed investigation of sub-seismic scale features related to salt diapirism. This work also demonstrates that individual cycles of passive and active diapirism may operate over timescales in the order of <30 ka during the growth of a diapir. In addition, individual unconformity-bound halokinetic sequences around the Sedom salt wall may last <40 ka, which is nearly an order of magnitude less than estimates of CHS

elsewhere, and is thought to reflect the rapid fluctuations in water level in the lacustrine environment.

Acknowledgements

GIA is grateful for funding from the Carnegie Trust for the Universities of Scotland that enabled fieldwork for this project. RW was supported by the Israel Science Foundation (ISF grant No. 1245/11). SM was supported by the Israel Science Foundation (ISF grant No. 1436/14). We would like to thank Chris Talbot and Yohann Poprawski for careful and constructive reviews. The authors appreciate the help of Nicolas Waldmann in precisely locating the positons of dated unconformities.

References

Aftabi, P., Roustaie, M., Alsop, G.I., Talbot, C.J., 2010. InSAR mapping and modelling of an active Iranian salt extrusion. J. Geol. Soc. Lond. 167, 155–170.
Agnon, A., Weinberger, R., Zak, I., Sneh, A., 2006. Geological Map of Israel. Sheet 20-I, II Sedom, Scale 1:50,000. Israel Geological Survey, Jerusalem.
Alsop, G.I., 1996. Physical modelling of fold and fracture geometries associated with salt diapirism. In: Alsop, G.I., Blundell, D.J., Davison, I. (Eds.), Salt Tectonics. Geological Society, 100. Special Publications, London, pp. 227–241.
Alsop, G.I., Jenkins, G., Davison, I., 1995. A preliminary study of drag zones adjacent to salt diapirs. In: Travis, C., et al. (Eds.), Salt, Sediment and Hydrocarbons, GCS-sepm Foundation Research Conference, pp. 1–10. Houston, Texas.
Alsop, G.I., Brown, J.P., Davison, I., Gibling, M.R., 2000. The geometry of drag zones adjacent to salt diapirs. J. Geol. Soc. Lond. 157, 1019–1029.
Alsop, G.I., Marco, S., 2012a. A large-scale radial pattern of seismogenic slumping towards the Dead Sea Basin. J. Geol. Soc. 169, 99–110.
Alsop, G.I., Marco, S., 2012b. Tsunami and seiche-triggered deformation within offshore sediments. Sediment. Geol. 261, 90–107.
Alsop, G.I., Marco, S., 2013. Seismogenic slump folds formed by gravity-driven tectonics down a negligible subaqueous slope. Tectonophysics 605, 48–69.
Alsop, G.I., Marco, S., 2014. Fold and fabric relationships in temporally and spatially evolving slump systems: a multi-cell flow model. J. Struct. Geol. 63, 27–49.
Alsop, G.I., Weinberger, R., Levi, T., Marco, S., 2015. Deformation within an exposed salt wall: recumbent folding and extrusion of evaporites in the Dead Sea Basin. J. Struct. Geol. 70, 95–118. http://dx.doi.org/10.1016/j.jsg.2014.11.006.
Al-Zoubi, A., Ten Brink, U.S., 2001. Salt diapirs in the Dead Sea basin and their relationship to quaternary extensional tectonics. Mar. Pet. Geol. 18, 779–797. http://dx.doi.org/10.1016/S0264-8172(01)00031-9.
Archer, S.G., Alsop, G.I., Hartley, A.J., Grant, N.T., Hodgkinson, R., 2012. Salt tectonics, sediments and hydrocarbon prospectivity. In: Alsop, G.I., Archer, S.G., Hartley, A.J., Grant, N.T., Hodgkinson, R. (Eds.), Salt Tectonics, Sediments and Prospectivity. Geological Society, vol. 363. Special Publications, London, pp. 1–6. http://dx.doi.org/10.1144/SP363.1.
Bartov, Y., Stein, M., Enzel, Y., Agnon, A., Reches, Z., 2002. Lake levels and sequence stratigraphy of Lake Lisan, the late Pleistocene precursor of the Dead Sea. Quat. Res. 57, 9–21.
Bornhauser, M., 1969. Geology of Day dome (Madison County, Texas) – a study of salt emplacement. Am. Assoc. Pet. Geol. Bull. 53, 1411–1420.
Burliga, S., 2014. Heterogeneity of folding in Zechstein (Upper Permian) salt deposits in the Klowdawa salt structure, central Poland. Geol. Q. 58, 565–576.
Butler, R.W.H., Maniscalco, R., Sturiale, G., Grasso, M., 2015. Stratigraphic variations control deformation patterns in evaporite basins: messinian examples, onshore and offshore Sicily (Italy). J. Geol. Soc. 172, 113–124. http://dx.doi.org/10.1144/jgs2014-024.
Callot, J.-P., Ribes, C., Kergaravat, C., Bonnel, C., Temiz, H., Poisson, A., Vrielynck, B., Salel, J.-F., Ringenbach, J.-C., 2014. Salt tectonics in the Sivas Basin (Turkey): crossing salt walls and minibasins. Bull. la Fr. 185, 33–42.
Davison, I., Alsop, I., Blundell, D., 1996a. Salt tectonics: some aspects of deformation mechanics. In: Alsop, G.I., Blundell, D.J., Davison, I. (Eds.), Salt Tectonics. Geological Society, vol. 100. Special Publications, London, pp. 1–10.
Davison, I., Bosence, D., Alsop, G.I., Al-Aawah, M.H., 1996b. Deformation and sedimentation around active Miocene salt diapirs on the Tihama Plain, northwest Yemen. In: Alsop, G.I., Blundell, D.J., Davison, I. (Eds.), Salt Tectonics. Geological Society, vol. 100. Special Publications, London, pp. 23–39.
Davison, I., Alsop, G.I., Evans, N.G., Safaricz, M., 2000a. Overburden deformation patterns and mechanisms of salt diapir penetration in the Central Graben, North Sea. Mar. Pet. Geol. 17, 601–618.
Davison, I., Alsop, G.I., Birch, P., Elders, C., Evans, N., Nicholson, H., Rorison, P., Wade, D., Woodward, J., Young, M., 2000b. Geometry and late-stage structural evolution of Central Graben salt diapirs, North Sea. Mar. Pet. Geol. 17, 499–522.
Dooley, T.P., Jackson, M.P.A., Jackson, C.A.-L., Hudec, M.R., Rodriguez, C., 2015. Enigmatic structures within salt walls of the Santos Basin-Part 2: mechanical explanation from physical modelling. J. Struct. Geol. 75, 163–187.
Farkash, L., Litman, H.L., Bloch, M.R., 1951. The formation of "salt tables" in natural and artificial solar pans. Res. Counc. Israel Bull. 1, 36–39.
Fossen, H., 2010. Structural Geology. Cambridge University Press, Cambridge, UK, p. 463.
Frumkin, A., 1996a. Uplift rate relative to base-levels of a salt diapir (Dead Sea basin, Israel) as indicated by cave levels. In: Alsop, G.I., Blundell, D.J., Davison, I. (Eds.), Salt Tectonics: Geological Society of London, vol. 100. Special Publication, pp. 41–47.
Frumkin, A., 1996b. Determining the exposure age of a karst landscape. Quat. Res. 46, 99–106. http://dx.doi.org/10.1006/qres.1996.0050.
Frumkin, A., 1996c. Structure of northern Mount Sedom salt diapir (Israel) from cave evidence and surface morphology. Israel J. Earth Sci. 45, 73–80.
Frumkin, A., 2009. Formation and dating of a salt pillar in Mount Sedom diapir, Israel. Geol. Soc. Am. Bull. 121, 286–293. http://dx.doi.org/10.1130/B26376.1.
Fuchs, L., Koyi, H., Schmeling, H., 2014. Numerical modeling on progressive internal deformation in down-built diapirs. Tectonophysics 632, 111–122.
Fuchs, L., Koyi, H., Schmeling, H., 2015. Numerical modelling of the effect of composite rheology on internal deformation in down-built diapirs. Tectonophysics 646, 79–95.
Gardosh, M., Kashai, E., Salhov, S., Shulman, H., Tannenbaum, E., 1997. Hydrocarbon exploration in the southern Dead Sea area. In: Niemi, T.M., Ben-Avraham, Z., Gat, J.R. (Eds.), The Dead Sea: the Lake and its Setting. Oxford University Press, Oxford, pp. 57–72.
Garfunkel, Z., 1981. Internal structure of the Dead Sea leaky transform (rift) in relation to plate kinematics. Tectonophysics 80, 81–108.
Giles, K.A., Rowan, M.G., 2012. Concepts in halokinetic-sequence deformation and stratigraphy. In: Alsop, G.I., Archer, S.G., Hartley, A.J., Grant, N.T., Hodgkinson, R. (Eds.), Salt Tectonics, Sediments and Prospectivity. Geological Society, vol. 363. Special Publications, London, pp. 7–31.
Haase-Schramm, A., Goldstein, S.L., Stein, M., 2004. U-Th dating of Lake Lisan aragonite (late Pleistocene Dead Sea) and implications for glacial East Mediterranean climate change. Geochim. Cosmochim. Acta 68, 985–1005.
Hatzor, Y.H., Heyman, E.P., 1997. Dilation of anisotropic rock salt: evidence from Mount Sedom diapir. J. Geophys. Res. 102, 14853–14868.
Hearon, T.E., Rowan, M.G., Giles, K.A., Hart, W.H., 2014. Halokinetic deformation adjacent to the deepwater Auger diapir, Garden Banks, 470, northern Gulf of Mexico: testing the applicability of an outcrop-based model using subsurface data. Interpretation 2 (4), SM57–SM76.
Hearon, T.E., Rowan, M.G., Lawton, T.F., Hannah, P.T., Giles, K.A., 2015a. Geology and tectonics of Neoproterozoic salt diapirs and salt sheets in the eastern Willouran Ranges, South Australia. Basin Res. 27, 183–207.
Hearon, T.E., Rowan, M.G., Giles, K.A., Kernen, R.A., Gannaway, C.E., Lawton, T.F., Fiduk, J.C., 2015b. Allochthonous salt initiation and advance in the northern Flinders and eastern Willouran ranges, South Australia: using outcrops to test subsurface-based models from the northern Gulf of Mexico. Am. Assoc. Pet. Geol. Bull. 99, 293–331.
Hudec, M.R., Jackson, M.P.A., 2011. The Salt Mine: a Digital Atlas of Salt Tectonics, vol. 99. The University of Texas at Austin, Bureau of Economic Geology, p. 305. Udden Book Series No. 5; American Association of Petroleum Geology Memoir.
Jackson, C.A.-L., Jackson, M.P.A., Hudec, M.R., Rodriguez, C., 2014. Internal structure, kinematics, and growth of a salt wall: insights from 3-D seismic data. Geology 42, 307–310. http://dx.doi.org/10.1130/G34865.1.
Jackson, C.A.-L., Jackson, M.P.A., Hudec, M.R., Rodriguez, C., 2015. Enigmatic structures within salt walls of the Santos Basin-Part 1: geometry and kinematics from 3D seismic reflection and well data. J. Struct. Geol. 75, 135–162.
Jackson, M.P.A., Vendeville, B.C., Schultz-Ela, D.D., 1994. Structural dynamics of salt systems. Annu. Rev. Earth Planet. Sci. 22, 93–117.
Johnson, H.A., Bredeson, D.H., 1971. Structural development of some shallow salt domes in Louisiana Miocene productive belt. Am. Assoc. Pet. Geol. Bull. 55, 204–226.
Kaufman, A., 1971. U-series dating of Dead Sea basin carbonates. Geochim. Cosmochim. Acta 35, 1269–1281. http://dx.doi.org/10.1016/0016-7037(71)90115-3.
Kernen, R.A., Giles, K.A., Rowan, M.G., Lawton, T.F., Hearon, T.E., 2012. Depositional and halokinetic-sequence stratigraphy of the Neoproterozoic Wonoka formation adjacent to Patawarta allochthonous salt sheet, Central flinders ranges, south Australia. In: Alsop, G.I., Archer, S.G., Hartley, A.J., Grant, N.T., Hodgkinson, R. (Eds.), Salt Tectonics, Sediments and Prospectivity. Geological Society, vol. 363. Special Publications, London, pp. 81–105.
Li, J., Webb, A.G., Mao, X., Eckhoff, I., Colon, C., Zhang, K., Wang, H., He, D., 2014. Active surface salt structures of the western Kuqa fold-thrust belt, northwestern China. Geosphere 10, 1219–1234. http://dx.doi.org/10.1130/GES01021.1.
Matmon, A., Fink, D., Davis, M., Niedermann, S., Rood, D., Frumkin, A., 2014. Unraveling rift margin evolution and escarpment development ages along the Dead Sea fault using cosmogenic burial ages. Quat. Res. 82, 281–295.
Nelson, T.H., 1991. Salt tectonics and listric normal faulting. In: Salvador, A. (Ed.), The Gulf of Mexico Basin. (The Geology of North America, Volume J). Geological Society of America, Boulder, Colorado, pp. 73–89.
Poprawski, Y., Basile, C., Agirrezabala, L., Jaillard, E., Gaudin, M., Jacquin, T., 2014. Sedimentary and structural record of the Albian growth of the Baikio diapir (the Basque Country, northern Spain). Basin Res. 26, 746–766. http://dx.doi.org/10.1111/bre.12062.
Ringenbach, J.-C., Salel, J.-F., Kergaravat, C., Ribes, C., Bonnel, C., Callot, J.-P., 2013. Salt tectonics in the Sivas Basin, Turkey: outstanding seismic analogues from outcrops. First Break 31, 93–101.
Rowan, M.G., 1995. Structural styles and evolution of allochthonous salt, Central Louisiana outer shelf and upper slope. In: Jackson, M.P.A., Roberts, D.G., Snelson, S. (Eds.), Salt Tectonics: a Global Perspective, vol. 65. AAPG Memoir, pp. 199–228.

Rowan, M.G., Lawton, T.F., Giles, K.A., Ratliff, R.A., 2003. Near-diapir deformation in La Popa basin, Mexico, and the northern Gulf of Mexico: a general model for passive diapirism. Am. Assoc. Pet. Geol. Bull. 87, 733–756.
Rowan, M.G., Lawton, T.F., Giles, K.A., 2012. Anatomy of an exposed vertical salt weld and flanking strata, La Popa Basin, Mexico. In: Alsop, G.I., Archer, S.G., Hartley, A.J., Grant, N.T., Hodgkinson, R. (Eds.), Salt Tectonics, Sediments and Prospectivity. Geological Society, vol. 363. Special Publications, London, pp. 33–57.
Salazar, J.A., Knapp, J.H., Knapp, C.C., Pyles, D.R., 2014. Salt tectonics and Pliocene stratigraphic framework at MC-118, Gulf of Mexico: an integrated approach with application to deep-water confined structures in salt basins. Mar. Pet. Geol. 50, 51–67.
Schofield, N., Alsop, I., Warren, J., Underhill, J.R., Lehne, R., Beer, W., Lukas, V., 2014. Mobilizing salt: magma-salt interactions. Geology 42, 599–602.
Schultz-Ela, D.D., Jackson, M.P.A., Vendeville, B.C., 1993. Mechanics of active salt diapirism. Tectonophysics 228, 275–312.
Schultz-Ela, D.D., 2003. Origin of drag folds bordering salt diapirs. Am. Assoc. Pet. Geol. Bull. 87, 757–780.
Smit, J., Brun, J.-P., Fort, X., Cloetingh, S., Ben-Avraham, Z., 2008. Salt tectonics in pull-apart basins with application to the Dead Sea Basin. Tectonophysics 449, 1–16.
Sneh, A., Weinberger, R., 2014. Major Structures of Israel and Environs, Scale 1: 50,000. Israel Geological Survey, Jerusalem.
Talbot, C.J., 1979. Fold trains in a glacier of salt in southern Iran. J. Struct. Geol. 1, 5–18.
Talbot, C.J., 1998. Extrusions of Hormuz salt in Iran. In: Blundell, D.J., Scott, A.C. (Eds.), Lyell: the Past Is the Key to the Present. Geological Society, vol. 143. Special Publications, London, pp. 315–334.
Talbot, C.J., Jackson, M.P.A., 1987. Internal kinematics of salt diapirs. AAPG Bull. 71, 1068–1093.
Torfstein, A., Haase-Schramm, A., Waldmann, N., Kolodny, Y., Stein, M., 2009. U-series and oxygen isotope chronology of the mid-Pleistocene Lake Amora (Dead Sea Basin). Geochim. Cosmochim. Acta 73, 2603–2630.
Trusheim, F., 1960. Mechanism of salt migration in northern Germany. Am. Assoc. Pet. Geol. Bull. 44, 1519–1540.
Vargas-Meleza, L., Healy, D., Alsop, G.I., Timms, N.E., 2015. Exploring the relative contribution of mineralogy and CPO to the seismic velocity anisotropy of evaporites. J. Struct. Geol. 70, 39–55. http://dx.doi.org/10.1016/j.jsg.2014.11.001.
Vendeville, B.C., Jackson, M.P.A., 1991. Deposition, extension and the shape of downbuilding salt diapirs. Am. Assoc. Pet. Geol. Bull. 75, 683.
Waldmann, N., 2002. The Geology of the Samra Formation in the Dead Sea Basin. MSc thesis. The Hebrew University of Jerusalem, p. 173.
Waldmann, N., Starinsky, A., Stein, M., 2007. Primary carbonates and Ca-Chlorided brines as monitors of palaeo-hydrological regime in the Dead Sea basin. Quat. Sci. Rev. 26, 2219–2228.
Waldmann, N., Stein, M., Ariztegui, D., Starinsky, A., 2009. Stratigraphy, depositional environments and level reconstruction of the last interglacial Lake Samra in the Dead Sea basin. Quat. Res. 72, 1–15.
Weinberger, R., 1992. Paleomagnetism in Mount Sedom, Israel: a Method to Determine the Structure of the Salt Body and to Reconstruct its Emergence from the Subsurface. M.Sc. Thesis. The Hebrew University of Jerusalem, p. 101 (in Hebrew, English abstract).
Weinberger, R., Agnon, A., Ron, H., 1997. Paleomagnetic reconstruction of a diapir emplacement: a case study from sedom diapir, the dead sea rift. J. Geophys. Res. 102, 5173–5192.
Weinberger, R., Begin, Z.B., Waldmann, N., Gardosh, M., Baer, G., Frumkin, A., Wdowinski, S., 2006a. Quaternary rise of the sedom diapir, dead sea basin. In: Enzel, Y., Agnon, A., Stein, M. (Eds.), New Frontiers in Dead Sea Paleoenvironmental Research, vol. 401, pp. 33–51. http://dx.doi.org/10.1130/2006.2401(03). Geol. Soc. Am. Special Paper.
Weinberger, R., Lyakhovsky, V., Baer, G., Begin, Z.B., 2006b. Mechanical modeling and InSAR measurements of Mount Sedom uplift, Dead Sea Basin: implications for rock-salt properties and diapir emplacement mechanism. Geochem. Geophys. Geosyst. 7, Q05014. http://dx.doi.org/10.1029/2005GC001185.
Weinberger, R., Bar-Matthews, M., Levi, T., Begin, Z.B., 2007. Late-Pleistocene rise of the Sedom diapir on the backdrop of water-level fluctuations of Lake Lisan, Dead Sea basin. Quat. Int. 175, 53–61. http://dx.doi.org/10.1016/j.quaint.2007.03.007.
Zak, I., 1967. The Geology of Mount Sedom [Ph.D. thesis]. The Hebrew University of Jerusalem, p. 208 (in Hebrew with an English abstract).
Zak, I., Freund, R., 1980. Strain measurements in eastern marginal shear zone of Mount Sedom salt diapir, Israel. AAPG Bull. 64, 568–581.
Zak, I., Karcz, I., Key, C.A., 1968. Significance of some sedimentary structures from Mount Sedom. Israel J. Earth Sci. 17, 1–8.
Zucker, C., 2014. The Deformation of the 'Salt Mirror' and the Uplift of Mount Sedom Salt Diapir, Israel. Msc. Thesis. The Hebrew University of Jerusalem, p. 63 (in Hebrew with an English abstract).